ANL/LWRS-23/1

Effect of thermal aging on microstructure and stress corrosion cracking behavior of Alloy 152 weldments

LWRS milestone Report Number: M3LW-23OR04020313

Nuclear Science and Engineering Division
Argonne National Laboratory

About Argonne National Laboratory
Argonne is a U.S. Department of Energy laboratory managed by UChicago Argonne, LLC under contract DE-AC02-06CH11357. The Laboratory's main facility is outside Chicago, at 9700 South Cass Avenue, Argonne, Illinois 60439. For information about Argonne and its pioneering science and technology programs, see www.anl.gov.

DOCUMENT AVAILABILITY

Online Access: U.S. Department of Energy (DOE) reports produced after 1991 and a growing number of pre-1991 documents are available free at OSTI.GOV (http://www.osti.gov/), a service of the US Dept. of Energy's Office of Scientific and Technical Information.

Reports not in digital format may be purchased by the public from the National Technical Information Service (NTIS):
U.S. Department of Commerce
National Technical Information
Service 5301 Shawnee Rd
Alexandria, VA 22312
www.ntis.gov
Phone: (800) 553-NTIS (6847) or (703) 605-6000
Fax: (703) 605-6900
Email: **orders@ntis.gov**

Reports not in digital format are available to DOE and DOE contractors from the Office of Scientific and Technical Information (OSTI):
U.S. Department of Energy
Office of Scientific and Technical Information
P.O. Box 62
Oak Ridge, TN 37831-0062
www.osti.gov
Phone: (865) 576-8401
Fax: (865) 576-5728
Email: **reports@osti.gov**

ANL/LWRS-23/1

Effect of thermal aging on microstructure and stress corrosion cracking behavior of Alloy 152 weldments

LWRS milestone Report Number: M3LW-23OR04020313

Bogdan Alexandreanu, Yiren Chen, Xuan Zhang and Wei-Ying Chen

Nuclear Science and Engineering Division, Argonne National Laboratory

September 2023

This page intentionally left blank

ABSTRACT

Nickel-based Alloy 690 and the associated weld Alloys 52 and 152 are typically used for nozzle penetrations in replacement heads for pressurized water reactor (PWR) vessels, because of their excellent overall resistance to general corrosion and environmental degradation, primarily stress corrosion cracking (SCC). However, many of the existing PWRs are expected to operate for 40-80 years. Likewise, water-cooled small modular reactors (SMRs) will use Ni-Cr alloys and are expected to receive initial operating licenses for 60 years. Hence, the thermal stability of Ni-Cr alloys is critical for the long-term performance of both existing and advanced nuclear power plants, and possibly spent fuel storage containers. The objective of this research is to understand the microstructural changes occurring in high-Cr, Ni-based Alloy 152 weldments during long time exposure to the reactor operating temperatures, and the effect of these changes on the service performance. One area of particular concern is the potential for long range ordering (LRO), *i.e.* formation of the intermetallic Ni_2Cr phase under prolonged exposure to reactor temperatures and/or irradiation, which can increase strength, decrease ductility, and cause dimensional changes or lead to in-service embrittlement of components made with these alloys. Hence, this research focused on the microstructural evolution and the SCC response of Alloy 152 under accelerated thermal aging. The materials studied involved three heats of Alloy 152 used to produce a dissimilar metal weld (DMW) joining an Alloy 690 plate to an Alloy 533 low alloy steel (LAS) plate, thermally aged at three different temperatures (370°C, 400°C and 450°C) for up to 75,000h (equivalent to 60 years of service). The microstructural characterization by means of synchrotron X-ray conducted in small, 0.2 mm - step line scans in the high-deformation regions of the weld root – covering areas spanning from the weld heat affected zone (HAZ) in Alloy 690 to the weld and weld butter on LAS - did not show evidence of LRO in any of the three Alloy 152 heats aged at 370°C and 450°C to an equivalent of 60 years of service. Testing in a primary water environment of two heats of Alloy 152 aged at 370°C to a 60-year service equivalent revealed a fatigue and corrosion fatigue crack growth responses similar to those measured on the un-aged alloys. However, the SCC CGR response of the aged samples appears to show a deterioration in performance, confirming our previous observation.

TABLE OF CONTENTS

LIST OF FIGURES

LIST OF TABLES

ABBREVIATIONS

ANL	Argonne National Laboratory
APS	Advanced Photon Source
ASTM	American Society for Testing and Materials
BPR	Back Pressure Regulator
BWR	Boiling Water Reactor
CGR	Crack Growth Rate
CL	Constant Load
CMTR	Certified Material Test Report
CSL	Coincident Site Lattice
CT	Compact Tension
DO	Dissolved Oxygen
DMW	Dissimilar Metal Weld
ECP	Electrochemical Potential
EDX	Energy Dispersive X-ray Spectroscopy
EPRI MRP	Electric Power Research Institute Materials Reliability Program
GBE	Grain Boundary Engineering
GTAW	Gas Tungsten Arc Welding
HAZ	Heat Affected Zone
HX	Heat Exchanger
IG	Intergranular
LAS	Low Alloy Steel
LWR	Light Water Reactor
NRC	Nuclear Regulatory Commission
PPU	Partial Periodic Unloading
PWR	Pressurized Water Reactor
PWHT	Post Weld Heat Treatment
PWSCC	Primary Water Stress Corrosion Cracking
SCC	Stress Corrosion Cracking
SEM	Scanning Electron Microscopy
SMAW	Shielded Metal Arc Welding
SS	Stainless Steel
S	Side
T	Transverse
TC	Thermocouple
TG	Transgranular
WOL	Weld Overlay
WPS	Weld Procedure Specification

ACKNOWLEDGMENTS

This research was supported through the U.S. Department of Energy's Light Water Reactor Sustainability program, Materials Research Pathway. Program manager: Dr. Xiang (Frank) Chen.

1 Introduction

Alloy 690 and the associated weld Alloys 52 and 152 are Nickel-based alloys with high Cr contents typically used for nozzle penetrations in replacement heads for pressurized water reactor (PWR) vessels, because of their increased resistance to stress corrosion cracking (SCC) relative to Alloys 600, 82, and 182 [1, 2]. Many of these reactors are expected to operate for 40-80 years. Likewise, advanced water-cooled small modular reactors (SMRs) will use these Ni-Cr alloys in their primary systems and are expected to receive initial operating licenses for 60 years. For spent fuel containers, the desired lifetime is 10,000 years. Hence, the thermal stability of Ni-Cr alloys is critical for the long-term performance of nuclear plants and possibly spent fuel storage containers.

One area of concern is that the long time exposure to reactor operating temperatures can result in long range ordering (LRO), *i.e.* formation of the intermetallic Ni_2Cr phase which can lead to in-service embrittlement of Ni-Cr components. Research with binary Ni-Cr model alloys [3] has found that LRO promotes SCC, with an SCC CGR 1,000x larger than the non-ordered version of the alloy. However, Fe plays a key role in the development of LRO. It is not clear at this time whether LRO occurs in commercial Ni-Cr alloys containing significant Fe. The addition of Fe was found to hinder LRO formation in Ni-Cr alloys [4].

Perhaps the most comprehensive study on LRO of Alloy 690 was conducted by Framatome/ EdF [5, 6]. One of the main findings of this study was that an Alloy 690 heat with 7.2 wt. % Fe requires 70,000 h to develop LRO at 420°C, while ordering had not occurred in Alloy 690 with 10.4 wt. % Fe aged for 70,000 h at the same temperature. 20% added cold-work was found to decrease the time to develop LRO slightly, to 60,000h. More recently, Huotilainen et al. found significant increases in hardness in two of the four heats aged up to 10,000h at 400°C [7]. The two heats that hardened had a lower Fe content than the heats that did not harden as a result of aging (9.53 and 9.3 wt. % vs. 10.37 and 10.04 wt. %). The latter observation is consistent with the formation of LRO as its kinetics is known to decrease with the increase of Fe concentration, however, Fe levels of up to 10 wt. % were found not to impede the LRO formation [4]. Nevertheless, the hardening reported in two of the four heats is similar to that resulting from 15-20% added cold work [7], thus, may have the potential to elevate their SCC susceptibility, leading to CGRs comparable to those typical of Alloy 600. Another remarkable recent study has found that LRO precipitation under proton irradiation was observed for the first time, in alloys C22, 625, 625P, 625D, 725, and 690 [8]. The Fe level in the Alloy 690 heat was 10.38 wt. %, and the irradiation was conducted at 360°C with 2 MeV protons to a damage level of 2.5 dpa.

Overall, the research to date on the effect of aging in Ni-based alloys seems to have been focused almost exclusively on the base alloys, and primarily on model alloys as the investigators sought to gain a fundamental understanding of the mechanisms in play. As a result, research on commercial heats has been extremely scarce and limited to microstructural examinations. As noted previously, with the notable exception of the study by Young et. al [3] on model alloy Ni-33Cr, the effects of those microstructural changes on the SCC response have not been evaluated.

The need for an assessment of the long-term aging effects on the performance in Alloy 690 and associated weldments was identified as a research gap in the Light Water Reactor Sustainability (LWRS) stakeholders report for 2020 [9], and was recognized as a strategic research need by both industry [2, 10] and regulators [11]. Hence, a research program was initiated at Argonne in 2020 to address that need and bridge the gap between the microstructural examination and performance testing. In order to study the effect of aging on performance, ANL produced an Alloy 152 dissimilar metal weld joining Alloy 690 and Alloy 533 LAS in 2011, identical to the one developed and produced for the US NRC program in 2010, which was then aged up to 75,000h over the following nine years, to 30 and 60-year service equivalents. This creates the opportunity to examine the effects of aging in several pedigreed alloys that have been characterized and tested extensively at ANL and worldwide in the un-aged condition over the past decade.

In its first year, the Argonne program focused on the microstructural evolution and the SCC response of Alloy 690 under accelerated thermal aging and irradiation conditions [12]. In addition to the aged Alloy 690, the study also involved specimens neutron-irradiated in the BOR-60 reactor up to 40 dpa. For aged Alloy 690 specimens, hardness was found to increase with aging time, however, the microstructural characterization by means of synchrotron X-ray did not find evidence of LRO. The microstructural characterization of neutron-irradiated specimens by TEM found no evidence of LRO either. Testing in a primary water environment of Alloy 690 specimens aged to a 60-year service equivalent revealed a fatigue and corrosion fatigue crack growth responses similar to those measured on the un-aged alloy. The SCC CGR response was also low. Overall, the two Alloy 690 heats investigated in this work, aged up to 60-year service equivalents or exposed to neutron irradiation up to 40 dpa, did not exhibit a deterioration in microstructure or performance.

The current research has been focused on the microstructural evolution and the SCC response of Alloy 152 under accelerated thermal aging. Two years ago, three weld heats aged at 370°C and 450°C equivalent to 60 years of service were analyzed by Synchrotron X-ray Diffraction (XRD), and no ordering was observed [13]. However, the SCC response of the 60-year aged specimen appeared to show a deterioration [13]. In order to confirm these findings, during the last year, a finer scan of XRD evaluation was conducted in the high-deformation root region of the weld covering areas spanning from the weld heat affected zone (HAZ) in Alloy 690 to the weld and weld butter on LAS. In order to confirm the SCC findings of two years ago, two additional Alloys 152 heats aged to a 60-year service equivalent were tested in a primary water environment.

Chapter 2 describes the weld mockup used in the aging study, including the materials of fabrication, the schematic design of the welds, and the weld fabrication processes. One of the objectives for this weldment was that the materials and welding parameters should be representative of those used for actual welds used in service. Chapter 2 also presents the equipment used in the microstructural examinations. The crack growth testing equipment and experimental approach are also presented. ANL generally followed a well-established testing protocol that has been employed for a number of years and was reported in previous ANL reports.

Chapter 3 provides findings of the microstructural examinations and the results of the crack growth rate tests. Complete CGR data sets are provided as a function of testing conditions, and presented as crack advance vs. time plots.

Chapter 4 provides a discussion of the testing results in the framework provided by the well-established fatigue and corrosion fatigue behavior for these alloys, as well as the industry-proposed disposition curves for crack growth [1]. Finally, Chapter 5 gives a summary of the main findings and conclusions.

2 Experimental

This section describes the alloys used in this study, the equipment used for microstructural analysis, the configuration of test specimens for crack growth rate (CGR) testing, and the CGR test apparatus and experimental approach.

2.1 Alloys

The alloys used in this work came from weldment that was aged to 30-year and 60-year service equivalents. Since the microstructural investigation was focused on LRO, a model alloy Ni-33Cr – with known susceptibility to LRO - was also included in the investigation.

2.1.1 Alloy 152 weld produced by ANL (Alloy 690 to Alloy 533 Grade B Joint)

The research presented in this report focuses on aged Alloy 152 which was part of a weldment, hence, for completeness, this section presents all the component materials and steps undertaken to produce the weldment.

The Alloy 690 (Heat NX3297HK12) was received from Nuclear Alloy Corp. in a plate form that was 6.4-cm (2.25-in.) thick x 7.6-cm (3-in.) wide x 86.4-cm (34-in.) long. The designation for the metallurgical condition of the as-received plate was MIL-DTL-24802. To reach this condition, the alloy was vacuum-induction-melted, electro-slag-remelted, hot-rolled, de-scaled, and annealed at 1038°C (1900°F) for 2 h, then air-cooled. The chemical composition provided by the vendor, as well as that determined at ANL by inductively-coupled plasma optical emission spectrometry (ICP-OES), is reported in Table 1.

Table 1 Chemical composition (wt. %) of Alloy 690 (Heat NX3297HK12) plate.

Alloy ID (Heat)	Analysis	C	Mn	Fe	S	P	Si	Cu	Ni	Cr	Ti	Nb	Co
A 690WC (NX3297HK12)	Vendor	0.03	0.20	9.9	<0.001	-	0.07	0.01	59.5	29.5	-	-	-
	ANL	0.04	0.33	8.53	0.001	0.003	0.02	0.04	59.67	30.82	0.47	0.01	<0.01

The Alloy 690 plate was used to produce a 3-inch thick Alloy 152 butt weld to SA-533 Gr B class 1 steel (Heat A5466-2 from the Midland reactor lower head [13]) buttered with Alloy 152 filler metal. The geometry of the joint is shown in Figure 1. The joint was designed with a straight edge on the Alloy 690 side to facilitate SCC CGR testing of the Alloy 690 heat affected zone (HAZ). The SMAW welding procedure was qualified to ASME Section IX by ANL Central Shops [15].

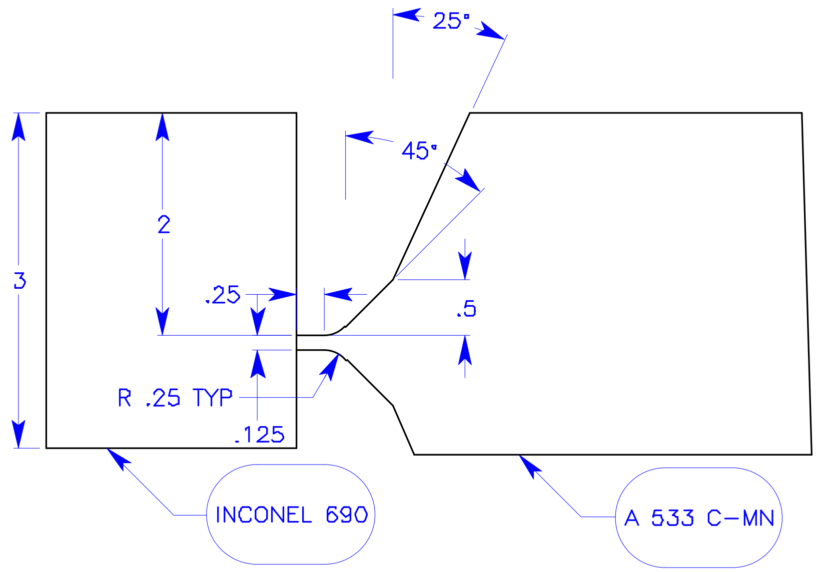

Figure 1 Joint design, Alloy 690 to SA-533 Gr B. Units are in inch.

2.1.1.1 Alloy 152 Weld Buttering

The LAS plate was machined with a bevel on one end. The beveled end was buttered with Alloy 152 F43 filler metal. A record was kept of the number and location of weld passes together with the heat code of the filler metal used, and the welding parameters that were used, Table 2 [15]. This record is shown in [15]. After each layer, a liquid penetrant (LP) check was performed. After buttering, the LAS piece was stress relieved at 1150 ± 25ºF for 3h. The chemical composition of the Alloy 152 filler heat 720129 that was used to produce the first layer of buttering is given in Table 3.

Table 2 Welding process and conditions for various weld passes used for fabricating the Alloy 152 butter

Weld Pass	Process	Filler Metal	Filler Size, in.	Heat Code	Type Polarity	Current, A	Voltage, V	Travel Speed, in./min	Notes
1 – 23	SMAW	Alloy 152, EniCrFe-7	1/8	720129	DCRP	97-102	21 – 23	5	Layer 1 LP
24-44	SMAW	Alloy 152, EniCrFe-7	5/32	146444	DCRP	113-117	25 – 26	5	Layer 2 LP
45-65	SMAW	Alloy 152, EniCrFe-7	5/32	146444	DCRP	113-117	25 – 26	5	Layer 3 LP

DCRP = direct current reverse polarity

Table 3 Chemical composition (wt. %) of Alloy 152 heats used to produce the weld buttering

Alloy ID	Analysis	C	Mn	Fe	S	P	Si	Cu	Ni	Cr	Ti	Nb+Ta	Co
A152 (720129)	CMTR	0.037	3.70	9.28	<0.001	<0.003	0.51	0.01	55.26	28.92	0.12	1.92	<0.01
A152 (146444)	CMTR	0.040	3.56	9.36	<0.001	<0.003	0.46	<0.01	55.25	29.04	0.15	1.84	<0.01

2.1.1.2 Alloy 152 Weldment

The buttered LAS piece described in the previous sub-section was beveled on the buttered edge leaving ¼" of Alloy 152 F43 weld material on the face, and a section of Alloy 690 plate was used to make the opposing part of the butt weld. A double bevel J-grove weld was produced according to the design shown in Figure 1, and the number and location of weld passes together with the heat code of the filler metal used, as well as the welding parameters are given in Table 4. The root pass of the weld and back grind was LP tested, and the final weld surface was also LP tested. The final weld was radiographed per ASME Section IX. The resulting weld along with its component heats is shown in Figure 2 and Figure 3. The chemical composition of the Alloy 152 filler heat WC04F6 that was used to complete the butt weld is given in Table 5.

Table 4 Welding process and conditions for various weld passes used for fabricating the A152 butt weld

Weld Pass	Process	Filler Metal	Filler Size, in.	Heat Code	Type Polarity	Current, A	Voltage, V	Travel Speed, in./min	Notes
1 – 8	SMAW	Alloy 152, EniCrFe-7	1/8	720129	DCRP	97-102	21 – 23	5	
9-14	SMAW	Alloy 152, EniCrFe-7	1/8	146444	DCRP	97-102	25 – 26	5	Root LP BG LP
15-26	SMAW	Alloy 152, EniCrFe-7	5/32	146444	DCRP	113-117	25 – 26	5	Final LP
27-76	SMAW	Alloy 152, EniCrFe-7	1/8	WCO4F6	DCRP	97-102	25 – 26	5	Final LP

DCRP = direct current reverse polarity

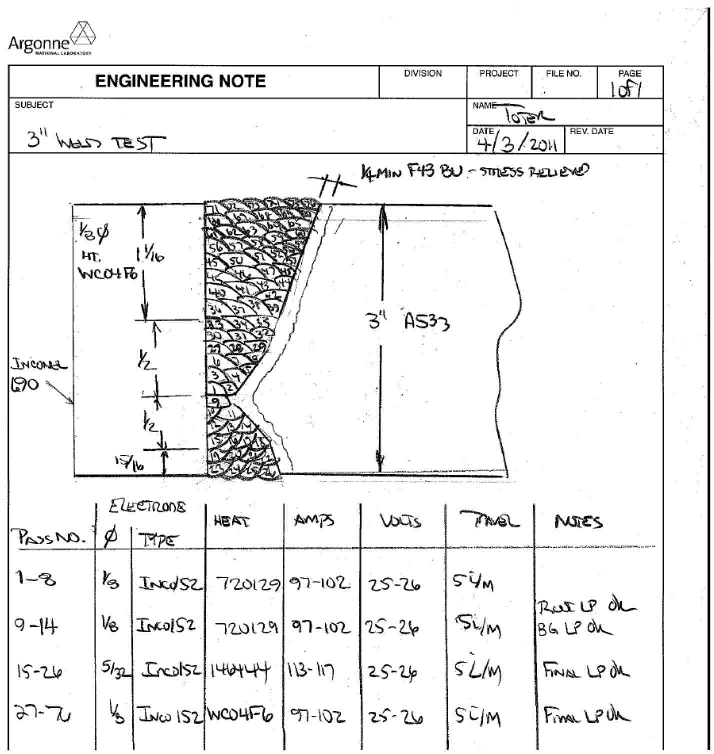

Figure 2 Schematic of the Alloy 152 weld joining Alloy 690 and Alloy 533 produced for aging in 2011. The weld was produced in an identical fashion using the same materials and procedures used to produce the weld for the US NRC program a year earlier. The table below the weld schematic shows the Alloy 152 weld heats and welding parameters.

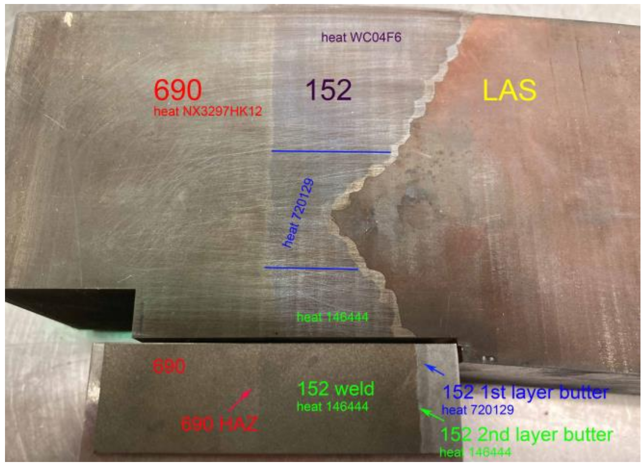

Figure 3 Alloy 152 weld joining Alloy 690 and Alloy 533 aged to a 60-year service equivalent. The three Alloy 152 weld heats are identified.

Table 5 Chemical composition (wt. %) of Alloy 152 heat WC04F6 used to complete the butt weld

Alloy ID (Heat)	Analysis	C	Mn	Fe	S	P	Si	Cu	Ni	Cr	Ti	Nb	Co
A152 (WC04F6)	CMTR	0.048	3.48	10.39	0.003	0.003	0.41	<0.01	55.20	28.70	0.09	1.54	<0.005
	ANL	-	3.88	9.56	-	<0.08	0.52	<0.04	53.70	28.40	0.10	1.80	<0.04

2.1.2 Prior characterization and testing of the un-aged Alloy 152 to Alloy 533 Grade B Joint

One of the main advantages of using the weldment described in this section for an aging study is the existence of a large database for benchmarking. The non-aged material from the sister weldment has been tested extensively at ANL under an US NRC program [16-18] and elsewhere. Some key findings are as follows:

Alloy 690:

- Alloy 690 Heat NX3297HK12 was the original material used by ANL in 2006 to show that 26% cold work promotes SCC growth in Alloy 690. The material was shared with several other laboratories and was tested extensively worldwide. Notably, 11% - the most from any one heat - of the data points in the MRP-386 database [2] were obtained using this heat. Alloy 690 Heat NX3297HK12 has a Fe content below 10 wt. % (9.9 and 8.53 wt. % in two independent measurements, Table 1), so it could be prone to developing LRO under long term exposure. However, the microstructural characterization conducted in this program by means of synchrotron X-ray did not find evidence of LRO in the specimens aged to 60 year of service equivalents [12]. Nevertheless, as described previously, aging to an 80-year service equivalent is in progress.

The Alloy 152 weldment was produced with three heats:

- Alloy 152 Weld Heat WC04F6 was used in the upper J-weld. It was tested extensively at ANL [16, 18] and elsewhere, and significant IG SCC was developed routinely in testing, resulting in moderately-high SCC CGRs, Figure 4. It is the most SCC-susceptible weldment in the MRP-386 database [2]. Alloy 152 Weld Heat WC04F6 has a Fe content of 10.39 wt. % (Table 5), so it would be less prone to the formation of LRO under long term exposure.

- Alloy 152 Weld Heat 720129 was used to weld on both sides of the root. It has not been tested as part of the weld, but was tested as the first buttering layer on Alloy 533 LAS. Alloy 152 Weld Heat 720129 has a Fe content of 9.28 wt. % (see Table 3), so it would be prone to LRO formation under long term exposure.
- Alloy 152 Weld Heat 146444 was used to complete the bottom J-weld. It has not been tested as part of the weld, but was tested as the second buttering layer on Alloy 533 LAS. Alloy 152 Weld Heat 146444 has a Fe content of 9.36 wt. % (see Table 3), so it would be prone to LRO formation under long term exposure.

The Alloy 152 butter was produced with two heats (Table 3):

- Alloy 152 Weld Heat 720129 was used as a first layer butter on Alloy 533 LAS. It has been tested extensively at ANL [17] and elsewhere. In SCC CGR testing, this weldment produced fully IG-engaged crack fronts, and very high rates, Figure 5 [17]. The weldment and tested specimens were examined extensively at ANL and worldwide. Alloy 152 Weld Heat 720129 has a Fe content of 9.28 wt. % (see Table 3), so it would be prone to LRO formation under long term exposure.
- Alloy 152 Weld Heat 146444 was used as a second layer butter on the Alloy 533 LAS and was tested in that configuration. This weldment was found to be resistant to SCC. Alloy 152 Weld Heat 146444 has a Fe content of 9.36 wt. % (see Table 3), so it would be prone to LRO formation under long term exposure.

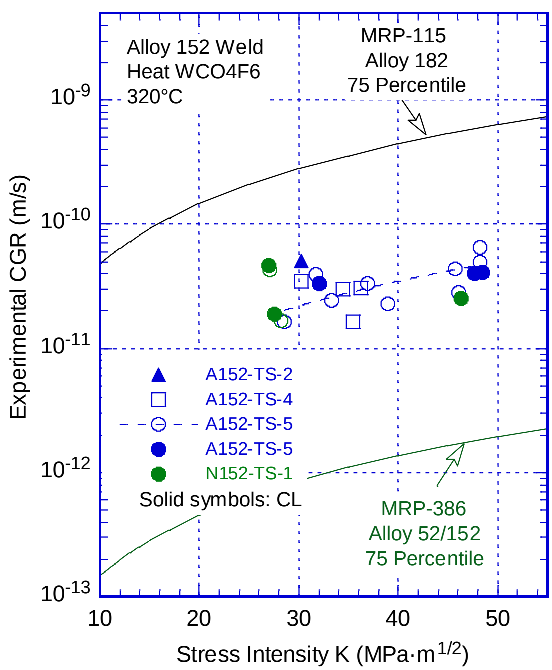

Figure 4 **SCC CGRs for Alloy 152 weld heat WC04F6 [16, 18]. Solid symbols represent SCC CGRs measured under constant load (CL) and open symbols represent SCC CGRs measured under periodic partial unloading (PPU) conditions. The proposed disposition curves for Alloys 182 [1] and 52/152 [2] are included.**

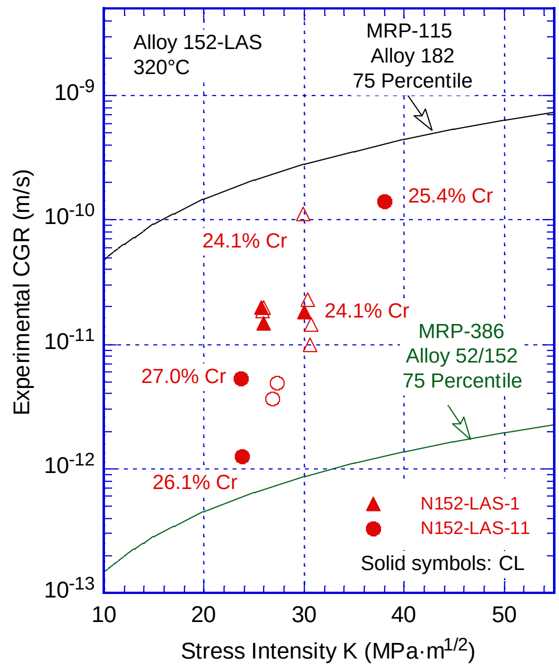

Figure 5 SCC CGRs for 1st layer of Alloy 152-LAS weld heat 720129 [17]. Cr-concentrations measured along the crack path in the regions where the rates were determined are shown in the figures. Solid symbols represent SCC CGRs measured under constant load (CL) and open symbols represent SCC CGRs measured under periodic partial unloading (PPU) conditions. The proposed disposition curves for Alloys 182 [1] and 52/152 [2] are included.

This weldment was also made available to collaborators from Korea, and the microstructure of the Alloy 152 weld, particularly the butter, was examined extensively in the non-aged and intermediate aged conditions [19, 20].

2.1.3 Aging of the Alloy 690 to Alloy 533 Grade B Joint

In order to emulate the thermal exposure at temperatures of 320°C during 30-year and 60-year service lifetimes of a component, this study employed an accelerated aging approach. The aging conditions were determined using the following equation:

$$\frac{t_{aging}}{t_{ref}} = \exp\left[-\frac{Q}{R}\left(\frac{1}{T_{ref}} - \frac{1}{T_{aging}}\right)\right] \quad (1)$$

where t_{aging} is the aging time (h), t_{ref} is the service time at operation temperature (h), T_{aging} is aging temperature (K), T_{ref} is operation temperature (K), R is the gas constant, and Q is the activation energy.

The 30-year and 60-year year service equivalents were estimated for three aging temperatures (370°C, 400°C, and 450°C) using Eq. (1) with an activation energy of 125 kJ/mol, in excellent agreement with the Framatome/EdF estimate for LRO formation [6], and the results are shown in Figure 6. The figure also includes a photograph of the actual aged weld pieces. The maximum accelerated aging temperature was 450°C to prevent the formation of microstructural phases atypical of normal operating conditions, such as excessive carbides or sigma phases. Specimens are designated by "temperature – service equivalent", for example specimen "400-Y60" was aged at a temperature of 400°C to reach a 60-year equivalent exposure at 320°C.

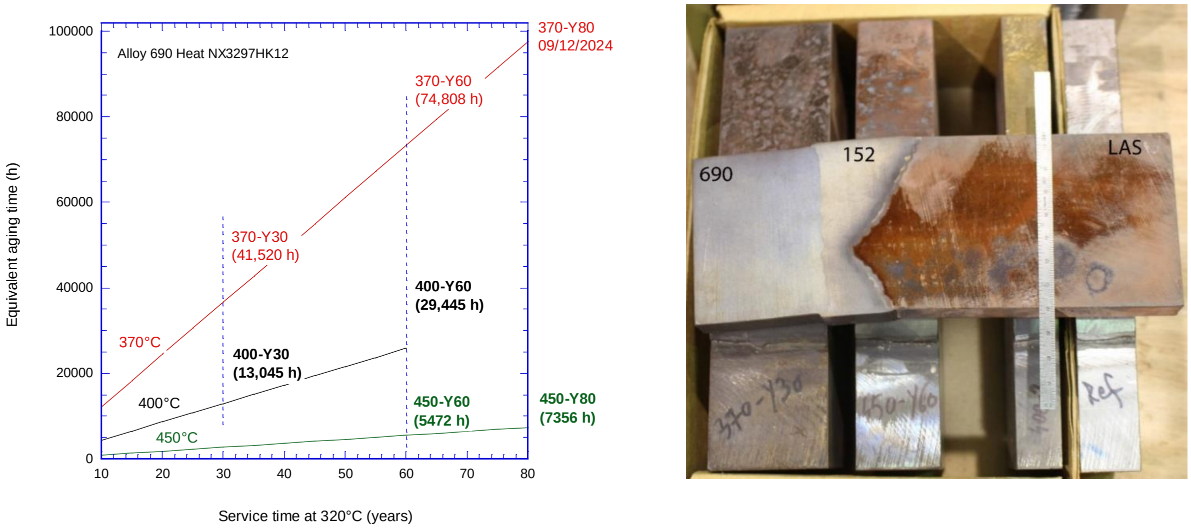

(a) (b)

Figure 6 **(a) Diagram showing the total hours for each aging temperature (370°C, 400°C, and 450°C). Estimates for 30-year and 60-year service equivalents calculated using Eq. (1) with an activation energy of 125 kJ/mol. The diagram also includes the actual aging times. Weld pieces are currently aged to 80-year service equivalent. (b) photograph of the actual pieces of Alloy 152 weld joining Alloy 690 and Alloy 533 that were aged.**

2.1.4 Model Ni-33Cr Alloy

Given that model alloys tend to develop LRO readily (see for example ref. [3]), a piece of model alloy with demonstrated LRO history [22] was obtained for this program from Dr. S.S. Kim of KAERI, Korea. The Ni-33Cr plate was made by vacuum induction melting followed by hot rolling at 1200°C, solution annealing at 1050°C for 1 h and water quenching. At ANL, this solution-annealed alloy was subjected to two different aging treatments at 475°C known to induce LRO [3]. The intent is to use these conditions as reference for the material characterization effort undertaken in this program which involves commercial heats.

2.2 Microstructural Characterization

The microstructural characterization involved hardness testing as well as analytical techniques such as synchrotron diffraction at ANL Advanced Photon Source (APS) focusing on detecting LRO.

2.2.1 X-ray Diffraction at Argonne APS

X-ray diffraction experiments were undertaken at ANL APS with the purpose of detecting LRO in aged Alloy 690 specimens. A similar evaluation has been undertaken previously at ANL APS on a model Ni-33Cr alloy where LRO occurs readily, in as little as 240h under thermal exposure of 475°C [22]. For example, Figure 7 (taken from ref. [22]) shows synchrotron X-ray diffraction peaks from Ni-33Cr alloy in water-quenched and aged conditions. The initial portions of the respective spectra are magnified and are shown as inserts in each figure. In addition to the expected FCC peaks that are present in all alloy conditions, figures (c) and (d) exhibit peaks - indexed with red – typical of Pt_2Mo-type domains. These Pt_2Mo superlattice peaks with d-spacings of 3.76 Å, 3.24 Å, and 2.38 Å were indexed as the (020), (011), and (110) of the body-centered orthorhombic (BCO) structure, and indicate the occurrence of Pt_2Mo-type ordering, i.e., LRO in aged samples.

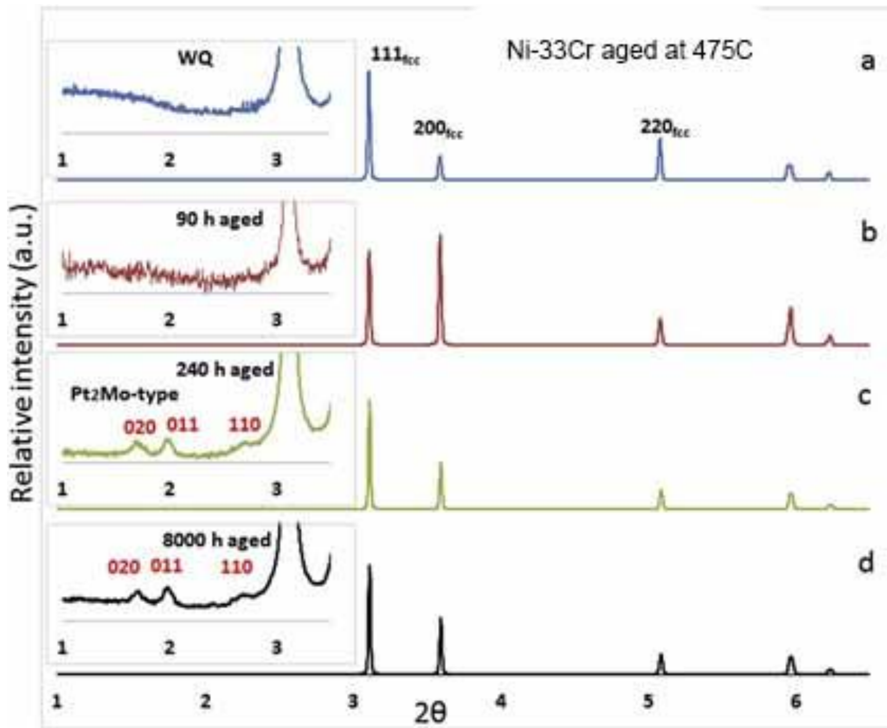

Figure 7 **Synchrotron X-ray peaks from Ni-33Cr alloy (a) water-quenched alloy (b) 90 h aged (c) 240 h aged (d) 8000 h aged. Initial portions of the respective spectra are magnified and are shown as insets. In addition to the FCC peaks that are present in all alloy conditions, (c) and (d) show peaks (indexed with red) from Pt_2Mo-type domains (taken from ref. [22]).**

For the present research, the X-ray diffraction experiment was performed at the 1-ID beamline of the APS, and the experimental details are summarized in Table 6. The detectors were calibrated with a CeO_2 powder sample (NIST standard SRM674b). All the samples were nominally 1-mm thick. For the weld samples, spot measurements were performed at the three Alloy 152 weld heats (refer to Figure 3). Figure 8 is a photo showing the actual beamline setup; note the three red marker dots on the sample plate indicating the measurement points on the three heats. At each measurement point, during the exposure, the sample rocked ±1.5°. This approach maximized the diffraction signal coverage in the azimuthal direction that the detector collected to create powder-like diffraction patterns for high-fidelity data analysis. A line scan was also performed for each weld sample, traveling from the Alloy 690 to the LAS with the thinnest weld section; in Figure 8 this corresponds to the right edge of the lead tape that was attached to the sample. For the Ni-33Cr model alloy samples, spot measurements were performed with the same ±1.5° rocking method. The 2D diffraction patterns were transformed into intensity maps of azimuth angles versus radial positions, and were integrated in the azimuthal direction to create the 1-D diffraction profiles for phase identification.

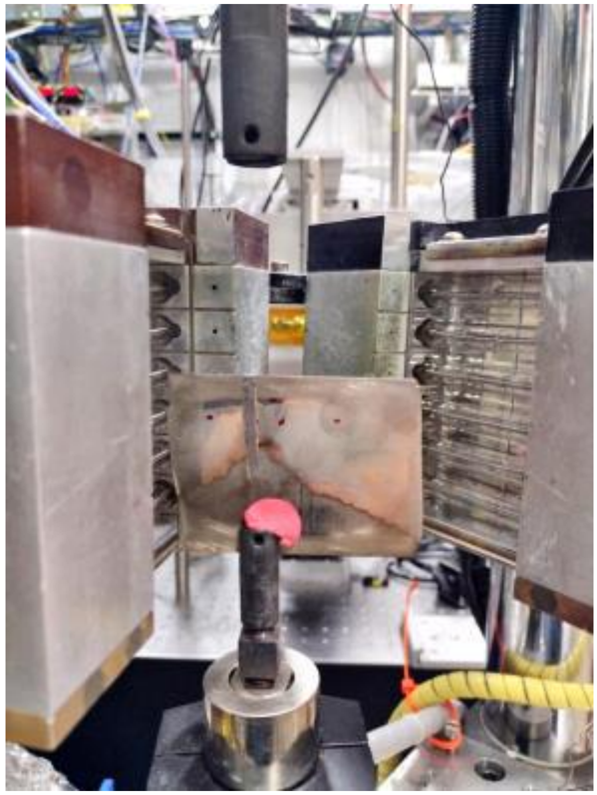

Figure 8 Experimental setup at the beamline for analyzing the weld material.

Table 6 Experimental details for the X-ray diffraction conductucted at ANL APS on aged Alloy 152 and Ni-33Cr specimens.

Material	Condition	X-ray Energy (keV)	Beam size (mm^2)	Distance sample-detector (mm)
A690 to LAS weld	reference	71.676	0.1 x 0.1	870
A690 to LAS weld	370°C-Y60	71.676	0.1 x 0.1	870
A690 to LAS weld	450°C-Y60	71.676	0.1 x 0.1	870
Ni-33Cr model alloy	reference	71.676	0.1 x 0.1	870
Ni-33Cr model alloy	475°C, 200h	71.676	0.1 x 0.1	870
Ni-33Cr model alloy	475°C, 2000h	71.676	0.1 x 0.1	870

2.3 SCC Crack Growth Rate Testing

2.3.1 Compact tension (CT) Specimens

The tests conducted under this project were performed on ½-T compact tension (CT) specimens; the geometry of the CT specimens is shown in Figure 9. The CGR tests were conducted in simulated PWR environments at 320°C. The testing protocol was in accordance with ASTM E-647, "Standard Test Method for Measurement of Fatigue Crack Growth Rates," [23] and ASTM E-1681, "Standard Test Method for Determining a Threshold Stress Intensity Factor for Environment-Assisted Cracking of Metallic Materials under Constant Load" [24].

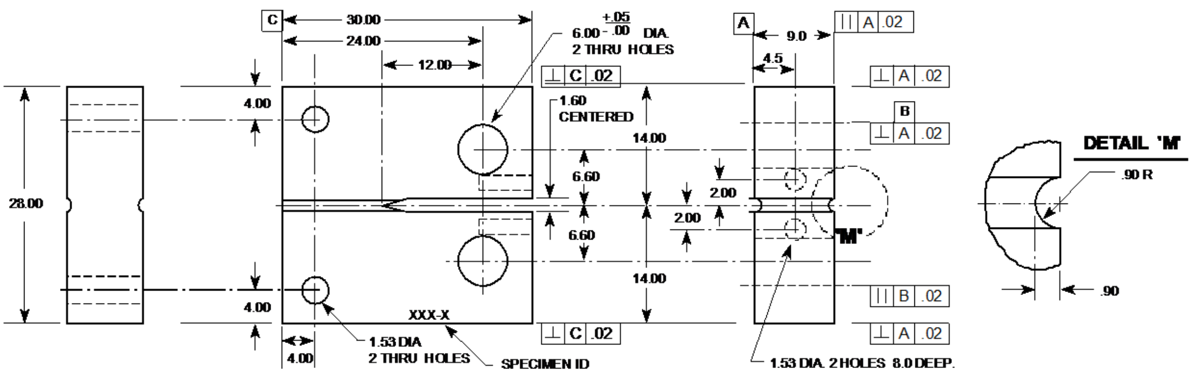

Figure 9 Configuration of the ½-T CT specimen used for this study. Dimensions are in mm.

2.3.2 PWSCC Crack Growth Test Facilities

The CGR tests were conducted in test facilities equipped with either 2 or 6-liter stainless steel (SS) autoclaves. Each system has a suite of calibrated instrumentation, including digitally controlled hydraulic loading and load cells, and an independent water loop to maintain a simulated PWR environment with water chemistry monitoring. The test systems are nearly identical except for the maximum load rating of the test frame and the volume of the autoclave vessel. A detailed description of the test system with the 2-liter autoclave is provided in this section.

The 2-liter autoclave test facility allows test temperatures of up to 350°C. Figure 10 is a photograph showing the entire test system. The servo-hydraulic test frame consists of a load train, an autoclave support frame, and autoclave. The hydraulic actuator is mounted on bottom of the test frame, with the load train components located above it. The load cell is located at the bottom of the pull rod. An Instron Model 8800 system is used to control the load on the specimen. The test temperature is maintained by heater bands mounted on the autoclave body.

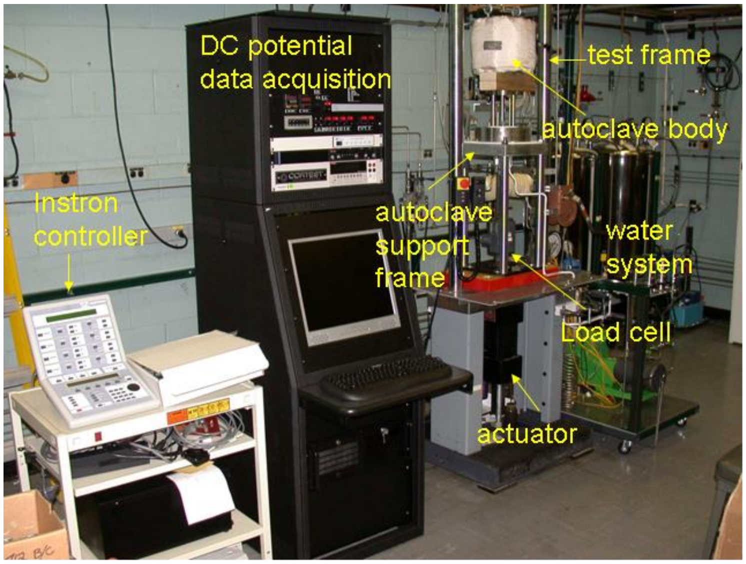

Figure 10 Layout of the 2-liter SCC test system.

The autoclave support frame consists of a thick plate supported by four compression rods (Figure 11). The internal load frame that contains the test specimen consists of a top plate supported by three rods. The upper two-piece clevis assembly is fastened to the top plate of the internal load frame, and the lower piece clevis assembly is connected to the pull rod. The specimen to be tested is mounted between the clevises. The specimen and clevises are kept electrically insulated from the load train by using oxidized Zircaloy pins and mica washers to connect the clevises to the rest of the load train. Water is circulated through a port in the autoclave head, which serves both as inlet and outlet. A schematic diagram of the recirculating water system is shown in Figure 12.

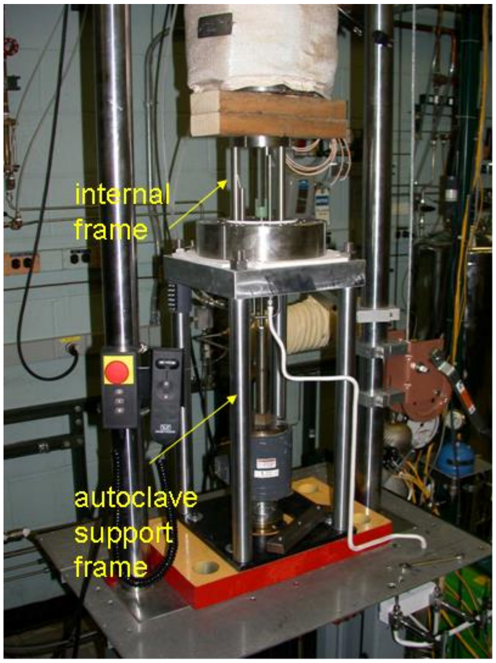

Figure 11 Photograph of the specimen load train for the 2-liter autoclave.

The simulated PWR feedwater contains 2 ppm Li as LiOH, 1000 ppm B as HBO_3, ≈2 ppm dissolved hydrogen (≈23 cm^3/kg), and less than 10 ppb dissolved oxygen (DO) [25]. Water is circulated at relatively low flow rates (15-25 mL/min). The test temperature was 320°C.

Crack extensions are monitored by the reversing-direct current (DC) potential difference method, Figure 13. In this method, a constant DC current is passed through the test specimen and the crack length is measured through the changes in the electrical voltage at the crack mouth. The electrical voltage measured across the crack mouth is related to the unbroken crack ligament resistance through the Ohm's law. Thus, as the crack advances, the length of the unbroken ligament decreases and its resistance increases. In short, as the crack advances the voltage measured across the crack mouth increases. Figure 13 shows a typical configuration of a CT specimen instrumented for crack growth measurements by the DC potential method: the current leads are welded on the top and bottom surfaces of the specimen, and potential leads are welded on the front face of the specimen across the machined notch but on diagonal ends. Also, to compensate for the effects of changes in resistivity of the material with time, an internal reference bar of the same material being tested is installed in series, near the test specimen. The voltage readings across the reference bar are used to normalize potential drop measurements for the CT test specimen. The changes in potential drop measurements for the CT test specimen are transformed into crack advance data using correlations developed for the specimen geometry that is tested. In practice, voltage readings are taken successively as the current is reversed, and, typically, 800 voltage readings are needed to generate 1 crack advance data point, approximately every 4 min. with a resolution of approximately 1-2 µm [0.039-0.079 mils].

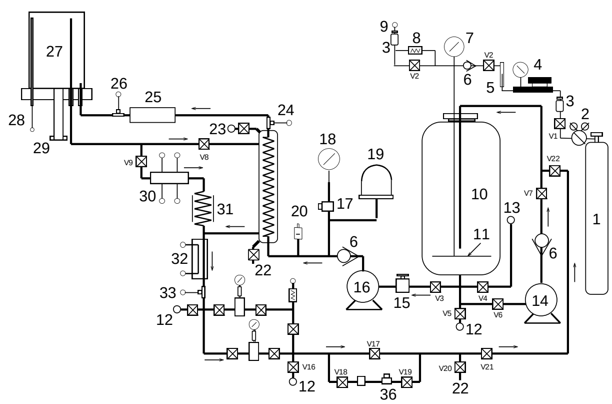

1. COVER GASS SUPPLY TANK
2. TWO-STAGE HIGH-PRESSURE REGULATOR
3. FLASH ARRESTOR
4. LOW-PRESSURE REGULATOR
5. FLOW METER
6. CHECK VALVE
7. COMPOUND VACUUM & PRESSURE GAUGE
8. PRESSURE RELIEF VALVE
9. VENT TO AIR & FLASH ARRESTOR
10. FEEDWATER STORAGE TANK
11. SPARGE TUBE
12. WATER SAMPLE PORT
13. FEEDWATER FILL PORT
14. FEEDWATER TANK RECIRCULATION PUMP
15. SOLENOID VALVE
16. HIGH-PRESSURE PUMP
17. PRESSURE TRANSDUCER
18. HIGH-PRESSURE GAUGE
19. ACCUMULATOR
20. RUPTURE DISC
21. HEAT EXCHANGER (HX)
22. DRAIN
23. SYSTEM BLEED PORT
24. HEAT EXCHANGER OUTLET TC
25. AUTOCLAVE PREHEATER
26. PREHEATER OUTLET TC
27. COMMERCIAL AUTOCLAVE
28. THERMOWELL
29. "BAL SEAL" RETAINER
30. ECP CELL
31. AIR-COOLED COIL
32. WATER COOLED HEAT EXCHANGER
33. BACK-PRESSURE REGULATOR (BPR) INLET TC
34. BPR
35. PH METER
36. CONDUCTIVITY METER

Figure 12 Schematic diagram of the recirculating 2-liter autoclave system.

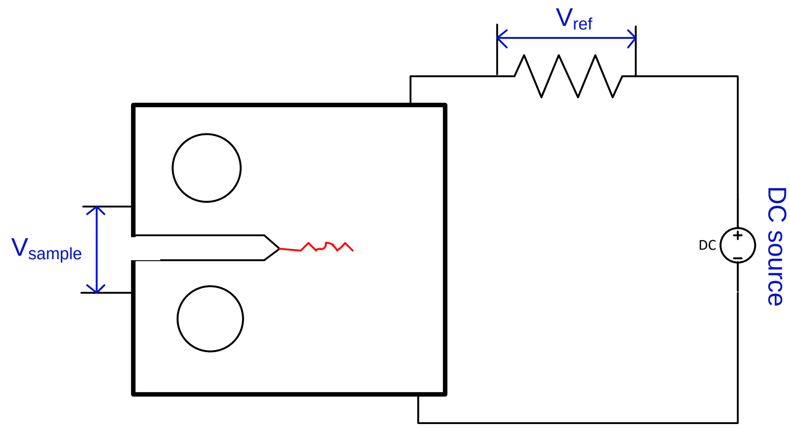

Figure 13 Principle of crack length measurement by the DC potential method.

3 Results

This section describes the findings of the hardness testing, microstructure examination by X-ray diffraction, and the results of SCC CGR testing in a primary water environment. The microstructural examinations focused on reference and weld heats aged at 370°C and 450°C equivalent to 60 years of service (conditions designated 370-Y60 and 450-Y60), Figure 14.

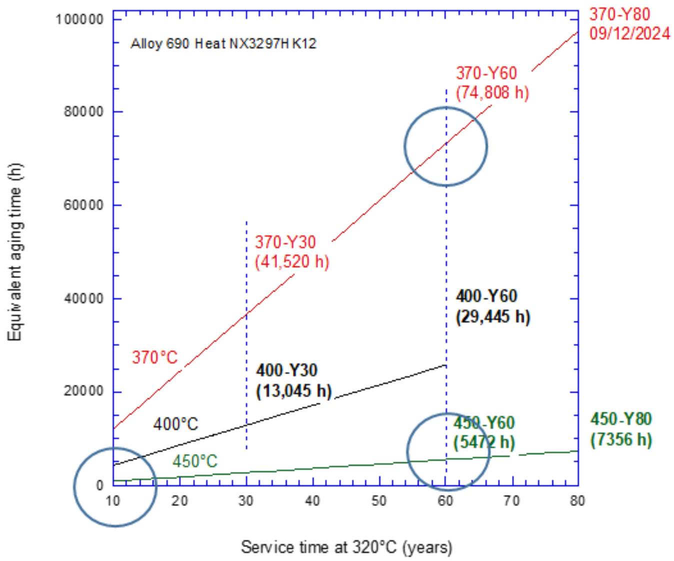

Figure 14 **Aging time equivalent vs. service time at 320°C. Conditions of high interest for the microstructural examination are indicated with circles.**

3.1 Microstructure

3.1.1 Hardness

The average hardness of the non-aged and two aged conditions - equivalent to 60 years of service, 370-Y60 and 450-Y60 - at select locations in the weld is shown in Figure 15. The load for all measurements was 100 gf, and the standard deviation for each sample hardness average shown in the figure is approximately 14 HV. The hardness map of the reference condition appears to show that the highest levels of deformation are in the weld root region. The overall figure shows similar average hardness values in the non-aged and aged conditions, with the possible exception of the weld root area where hardness appears to increase slightly with aging. The aging temperature, 370°C or 450°C, does not seem to affect the findings. The causes for the hardening – either Cr carbide precipitation or LRO – are both known to increase susceptibility to SCC.

From an SCC susceptibility standpoint, it is also worthy to note the apparently high levels of deformation in the LAS HAZ, although they are not the focus of the current investigation.

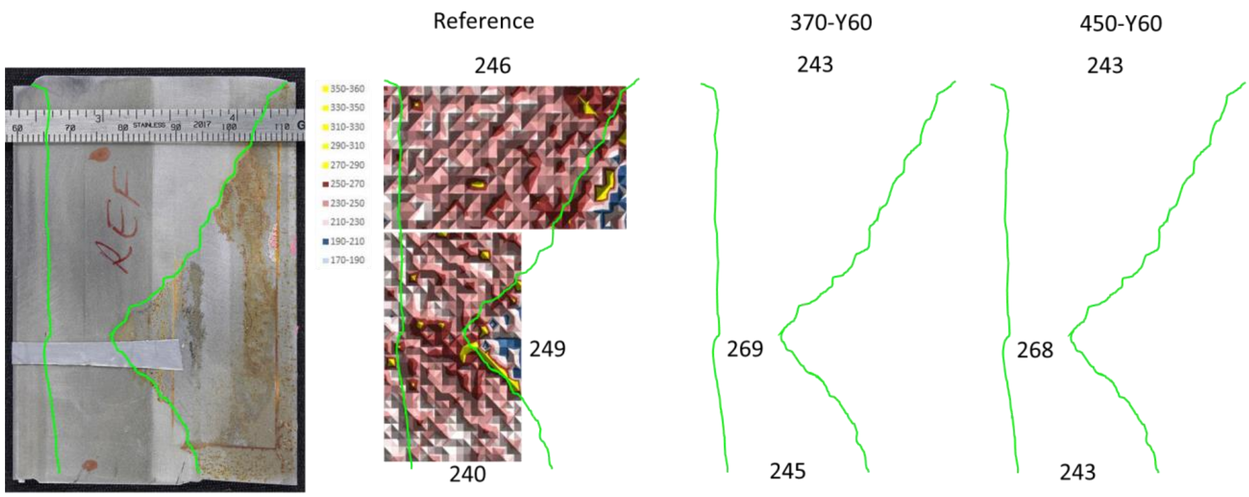

Figure 15 **Average hardness at select locations in the weld for non-aged and two aged conditions equivalent to 60 years of service, 370-Y60 and 450-Y60. The standard deviation for each sample hardness average shown in the figure is approximately 14 HV.**

3.1.2 X-ray Diffraction at Argonne APS

The three Alloy 152 heats - WC04F6, 720129, and 146444 - aged at 370°C and 450°C equivalent to 60 years of service (conditions 370-Y60 and 450-Y60) were examined by X-ray Diffraction (XRD) previously and were found not to display LRO [13]. In order to confirm these findings, and acknowledging the heterogeneity of weldments in in both chemistry and residual stress, it was decided to conduct a "finer" investigation with small step line scans in the weld root region of the weld, known for its high stress.

In the current investigation, Figure 16, the reference non-aged condition and the two 60-year aged conditions were evaluated by Synchrotron XRD for LRO over a region spanning areas from the weld HAZ in Alloy 690 to the weld and weld butter on LAS – see green arrow.

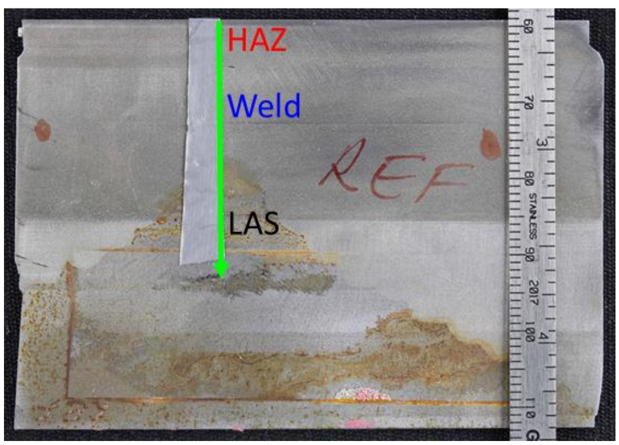

Figure 16 **XRD scanning at with 0.2 mm step was conducted in the weld root region – along the green arrow - spanning the Alloy 690 HAZ, weld rood, and Alloy 152 weld butter deposited on LAS.**

Figure 17 presents the results of this investigation. Aged model Ni-33Cr alloy with known LRO [12] was included for reference in Figure 17a. For the model alloy, in addition to the FCC peaks that are present in all conditions, the aged conditions show peaks - highlighted with green - from Pt_2Mo-type domains. These superlattice peaks with d-spacings of 3.76 Å and 3.24 Å were indexed as the (020) and (011) of the BCO structure, indicating Pt_2Mo-type ordering in these two samples. For the reference and 60-year aged conditions (Figure 17b-d), the XRD line scans conducted along the green arrow Figure 16 spanned a range of alloys in succession (top to bottom): Alloy 690 NX3297HK12 HAZ, Alloy 152 heat 720129 weld, Alloy 152 heat 146444 2nd layer butter, Alloy 152 heat 720129 1st layer butter, and Alloy 533 LAS. For ease of identification, these alloys are color coded as such: red for Alloy 690, blue for Alloy 152 weld, and black for the LAS. The absence of superlattice peaks with d-spacings of 3.24 Å indexed as the (011) of the BCO structure (see Figure 17a for comparison), suggests that the Pt_2Mo-type ordering has not occurred in any of these alloys.

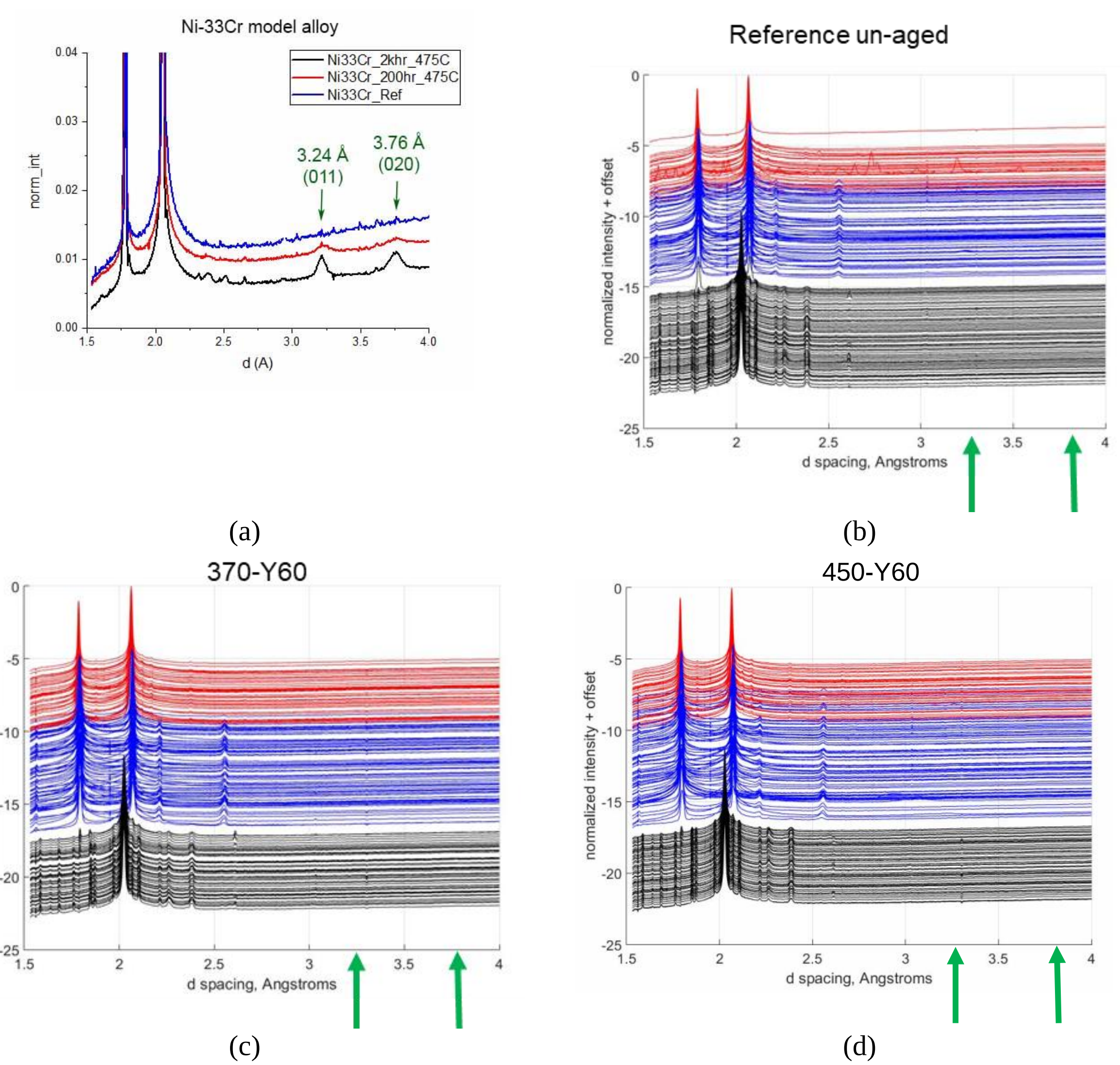

Figure 17 **Synchrotron X-ray peaks from (a) Ni-33Cr alloy, (b) reference un-aged weld, and 60-year aged equivalent conditions (c) 370-Y60, and (d) 450-Y60. Only the aged conditions of model alloy Ni-33Cr show peaks (indexed with green) consistent with Pt_2Mo-type domains.**

3.2 PWSCC Crack Growth Rate Testing

3.2.1 Location of SCC CGR test specimens in aged materials and prior results

The SCC testing of aged specimens involves specimens and heats that have already been tested in the as-welded condition, and have already shown increased susceptibility to SCC, Figure 4 and Figure 5. The SCC CGR testing of aged material is conducted on 1/2T CTs to accommodate more specimens and regions of interest. As such, as shown in Figure 18, from one "slice" of aged weld (370-Y60, aged at 370°C for 74,808 h – equivalent to 60 years of service), an Alloy 152 heat WC04F6 (top left) specimen, two Alloy 152 heats 720129 and 146444 in succession (bottom) specimen, and an Alloy 152 heat 720129 in a 1st layer configuration specimen were machined.

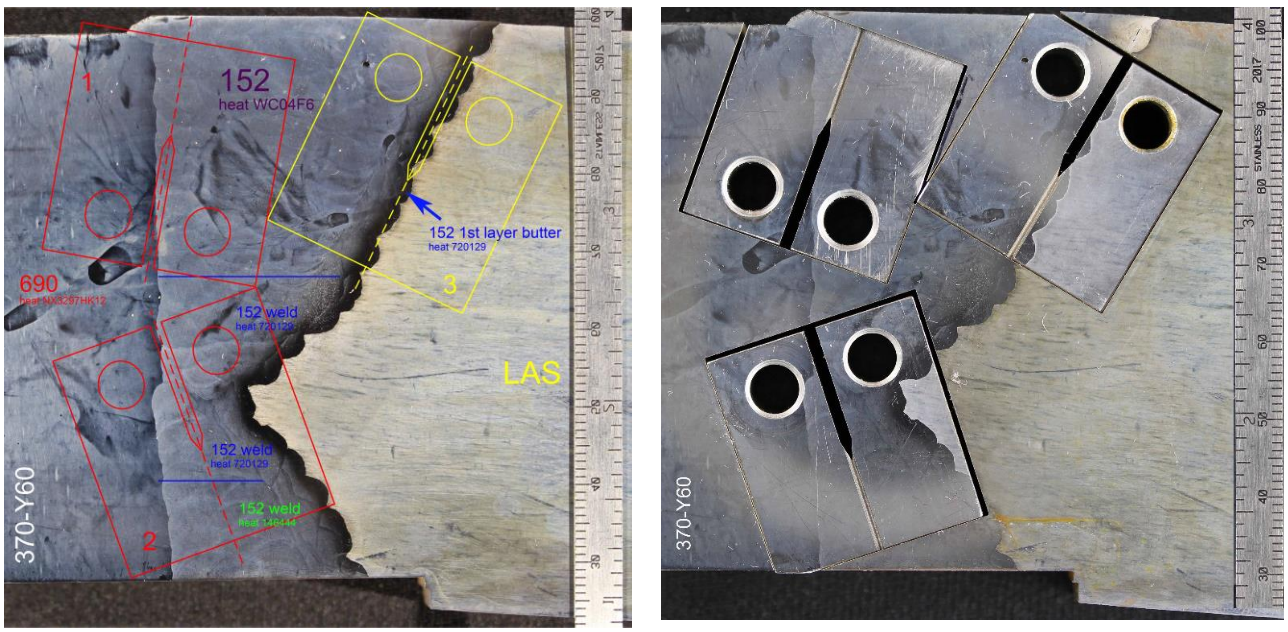

(a) (b)

Figure 18 a) Compact tension (CT) specimens designed to test the Alloy 152 heat WC04F6 (top left), Alloy 152 heats 720129 and 146444 in succession (bottom), and Alloy 152 heat 720129 in a 1st layer configuration. (b) CT specimens ready to be tested.

The specimen tested previously was the Alloy 152 heat WC04F6 (top left, specimen "1"), and was designated 370-Y60 N152. Figure 19 summarizes the results of that test and is included here for completeness. Figure 19a presents the cyclic CGR data obtained on Alloy 152 heat WC04F6 in the as-welded and aged conditions. In the figure, the cyclic CGRs measured in the environment are plotted vs. the CGRs predicted in air under the same loading conditions for Ni-based weldments. In this representation, the environmental enhancement, i.e., the departure from the "1:1 diagonal" can be easily visualized. Correlations describing cyclic CGRs in air and LWR environments have been established by ANL for Alloy 600, 690, Ni-base weldments as well as SSs [27-31]. For comparison, the expected cyclic CGR curve for Alloy 182 weld was also included. Figure 19a shows that, as expected, the cyclic CGRs in the mechanical fatigue regime (10^{-8}-10^{-7} m/s) are along the first diagonal, and that is true for both aged and un-aged specimens. Likewise, in the corrosion fatigue regime (10^{-11}-10^{-9} m/s), there is no difference between the aged and non-aged specimens. Also, unsurprisingly, at the lower end of the spectrum, the environmental enhancement of all Alloy 152 specimens is lower than the Alloy 182 curve – likely an effect of the higher Cr content. Figure 19b presents the SCC CGR data for the Alloy 152 heat WC04F6 in the non-aged [16, 18] and aged conditions vs. stress intensity factor, K. For context, the proposed disposition curves for Alloys 182 [1] and 52/152 [2] are included in the figures. The data comparison seems to suggest that aging to 60-year service equivalent appears to have a negative effect on the SCC resistance of this Alloy 152 heat. The EPRI MRP-386 [2] proposed disposition curve does not seem to bound any of the SCC CGR for this weld heat, in either non-aged or aged conditions.

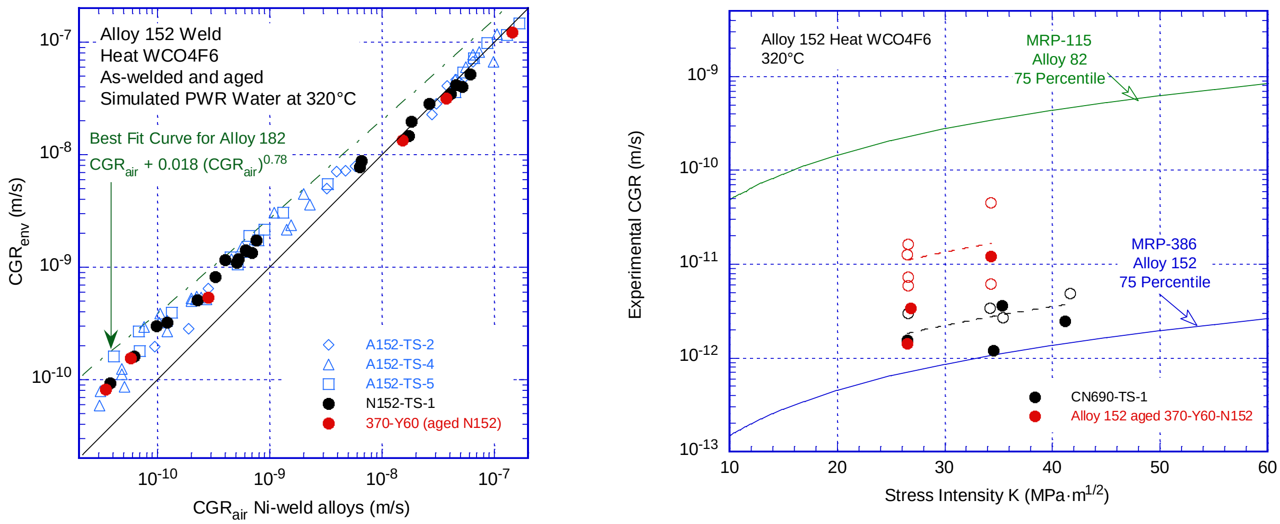

(a) (b)

Figure 19 **(a) Cyclic CGRs measured in the environment vs. CGRs predicted in air under the same loading conditions, and (b) SCC CGRs for Alloy 152 weld heat WC04F6 in the as- received [16, 18], and aged conditions. For SCC CGRs, solid symbols represent measurements under constant load (CL) and open symbols represent measurements under periodic partial unloading (PPU) conditions. The proposed disposition curves for Alloys 182 [1] and 52/152 [2] are included.**

3.2.2 Crack growth rate testing of Alloy 152 Specimen 370-Y60 N152-2W, aged at 370°C for 74,808 h

As described previously, to substantiate the finding of the SCC CGR test from two years ago, another specimen with two aged Alloy 152 heats - 720129 and 146444, specimen “2” in Figure 18 – was tested over the past year. As Figure 20 shows, the CGR test was initiated in Alloy 152 heat 720129, several SCC CGR determinations were made, then the crack was advanced in fatigue more than 2.34 mm away from the notch into Alloy 152 heat 146444, and the SCC CGR measurements were repeated. As described in section 2.1.2, non-aged Alloy 152 heat 720129 was only tested as a 1st layer weld butter on LAS, however, for Alloy 152 heat 146444, SCC CGR results for the non-aged condition are available for comparison in the EPRI MRP-386 database [2].

The testing conditions for this specimen are given in Table 7, and the changes in crack length and K_{max} with time are shown in Figure 21. Correlations describing cyclic CGRs in air (CGR_{air}) have been established by ANL for Alloy 600, 690, Ni-base weldments as well as SSs [27-31]. The test was initiated Alloy 152 heat 720129 in simulated primary water at 320°C with in-situ precracking (Pre a –

Pre b), and was followed by transitioning (test periods 1-3). The SCC CGR component evaluated by superposition in test periods 2 and 3 was 1.3 x 10^{-11} m/s, and the subsequent the response under constant load in period 4 was close to that value at 8.5 x 10^{-12} m/s. The SCC CGR component evaluated by superposition in test periods 5 and 6 was similar, suggesting that the crack tends to go off-plane. The crack was advanced to a different microstructure at a higher stress intensity factor, re-transitioned but the one SCC CGR determination under constant load was low despite SCC CGR component evaluations from cycle + hold in the low-10^{-11} m/s range, but decreasing, thus suggesting another case of off-plane cracking. In the interest of time, it was decided to advance the crack into the second Alloy 152 heat 146444. This was accomplished in test periods 15-19, then the crack was re-transitioned in test period 20-22. Environmentally-enhanced conditions were re-established at K=33 MPa $m^{1/2}$ to matched those for the non-aged specimen of Ref. [2,] and several SCC CGR components in the low-10^{-11} m/s range were evaluated by superposition in test periods in test period 22-26. Finally, the SCC CGR was measured under constant load in test period 27, and the result, 8.5 x 10^{-12} m/s, was close to the evaluations by superposition.

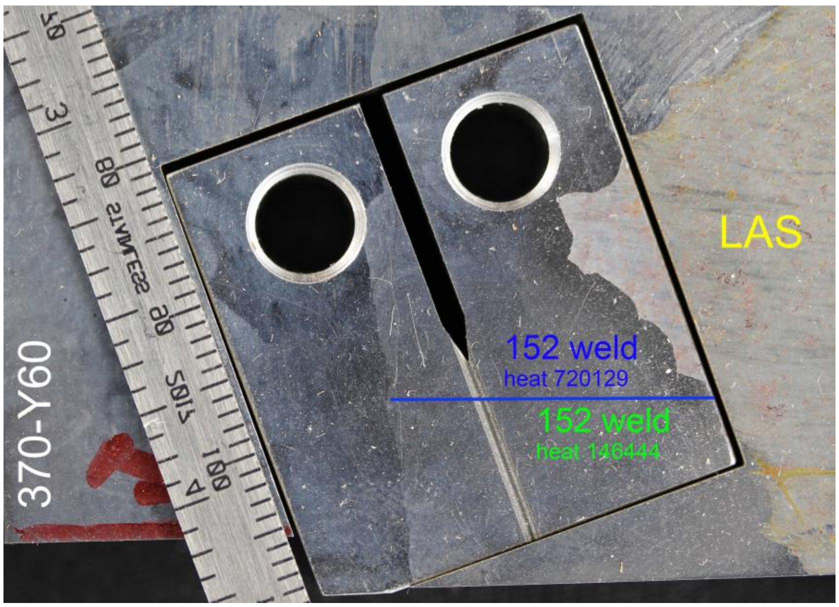

Figure 20 CT specimen 370-Y60 N152-2W used to test two aged Alloy 152 heats in succession. Aged condition 370-Y60 designated aging at 370°C for 74,808 h – equivalent to 60 years of service.

Table 7 Crack growth data in PWR water[a] for Alloy 152 Specimen 370-Y60 N152-2W aged for 74,808 h at 370°C

Test Period	Test Time, h	Temp., °C	Load Ratio R	Rise Time, s	Down Time, s	Hold Time, s	K_{max}, MPa·$m^{1/2}$	ΔK, MPa·$m^{1/2}$	CGR_{env}, m/s	Estimated CGR_{air}, m/s	Crack Length, mm
Pre a	5	320.4	0.30	1	1	0	26.8	18.7	6.81E-08	8.54E-08	12.106
Pre b	7	320.3	0.30	5	5	0	26.7	18.7	1.68E-08	1.69E-08	12.159
1	24	320.1	0.50	120	12	0	27.1	13.5	6.48E-10	3.22E-10	12.200
2	51	320.2	0.50	600	12	0	26.9	13.4	1.72E-10	6.26E-11	12.215
3	96	320.2	0.50	600	12	7,200	27.1	13.5	2.01E-11	4.96E-12	12.221
4	433	320.2	1.00	0	0	0	27.1	0.0	8.47E-12	-	12.228
5	509	320.1	0.50	600	12	7,200	27.2	13.6	1.69E-11	5.02E-12	12.233

Table 7 (cont.)

Test Period	Test Time, h	Temp., °C	Load Ratio R	Rise Time, s	Down Time, s	Hold Time, s	K_{max}, MPa·m$^{1/2}$	ΔK, MPa·m$^{1/2}$	CGR_{env}, m/s	Estimated CGR_{air}, m/s	Crack Length, mm
6	511	320.4	0.30	1	1	0	28.2	19.7	8.19E-08	1.06E-07	12.492
7	528	320.3	0.30	50	50	0	28.5	20.0	3.06E-09	2.22E-09	12.592
8	531	320.4	0.30	1	1	0	31.0	21.7	1.09E-07	1.56E-07	13.189
9	533	320.7	0.50	120	12	0	31.0	15.5	1.10E-09	5.64E-10	13.215
10	600	320.0	0.50	600	12	0	31.4	15.7	2.10E-10	1.18E-10	13.286
11	672	320.1	0.50	600	12	7,200	31.5	15.8	3.34E-11	9.21E-12	13.297
12	742	320.4	1.00	0	0	0	31.5	0.0	no growth	-	13.297
13	838	320.6	0.50	600	12	7,200	31.5	15.7	2.29E-11	9.21E-12	13.305
14	957	320.8	0.50	12	12	7,200	31.4	15.7	1.72E-11	9.96E-12	13.313
15	965	321.6	0.30	1	1	0	26.8	18.8	6.81E-08	8.70E-08	13.663
16	980	321.5	0.30	50	50	0	26.1	18.3	2.90E-09	1.57E-09	13.749
17	983	321.2	0.30	1	1	0	26.6	18.6	7.34E-08	8.43E-08	13.904
18	984	321.2	0.30	50	50	0	26.7	18.7	2.96E-09	1.70E-09	13.927
19	988	322.2	0.30	1	1	0	26.9	18.8	8.26E-08	8.86E-08	14.352
20	1,005	321.5	0.50	120	12	0	27.2	13.6	9.02E-10	3.33E-10	14.415
21	1,012	321.3	0.50	600	12	0	27.3	13.6	1.86E-10	6.71E-11	14.420
22	1,077	321.5	0.50	600	12	7,200	27.3	13.6	2.02E-11	5.17E-12	14.427
23	1,150	320.6	0.50	12	12	7,200	27.3	13.7	1.49E-11	5.60E-12	14.431
24	1,172	320.5	0.50	600	12	0	33.0	16.5	4.36E-10	1.45E-10	14.469
25	1,251	320.5	0.50	600	12	7,200	33.2	16.6	2.52E-11	1.14E-11	14.485
26	1,580	320.8	0.50	12	12	7,200	33.1	16.6	2.00E-11	1.23E-11	14.506
27	2,084	320.5	1.00	0	0	0	33.0	0.0	8.50E-12	-	14.516

[a]Simulated PWR water with 2 ppm Li, 1000 ppm B, and 2 ppm H. DO<10 ppb. Conductivity is 21±3 μS/cm, and pH is 6.4.

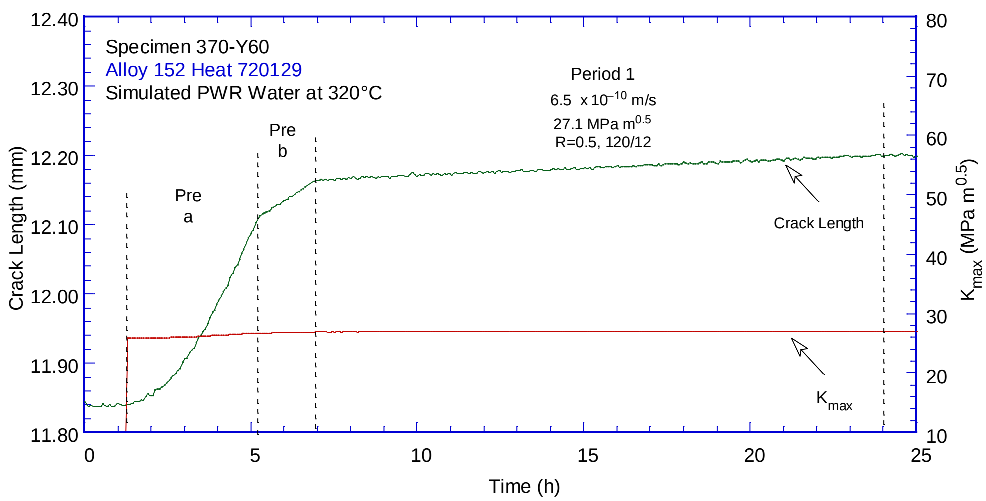

(a)

Figure 21 **Crack length vs. time in simulated PWR environment for Alloy 152 Specimen 370-Y60 N152-2W aged for 74,808 h at 370°C, during test periods: (a) precracking-1, (b) 2-5, (c) 10-14, (d) 20-26, and (e) 27.**

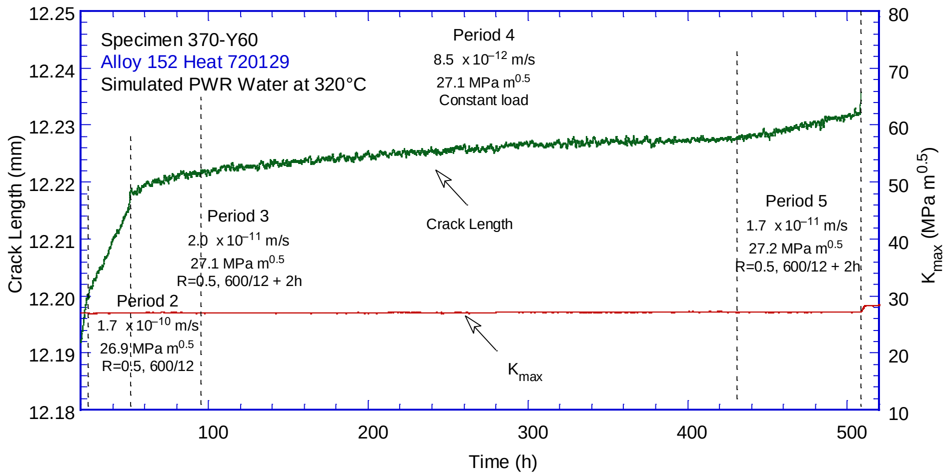

(b)

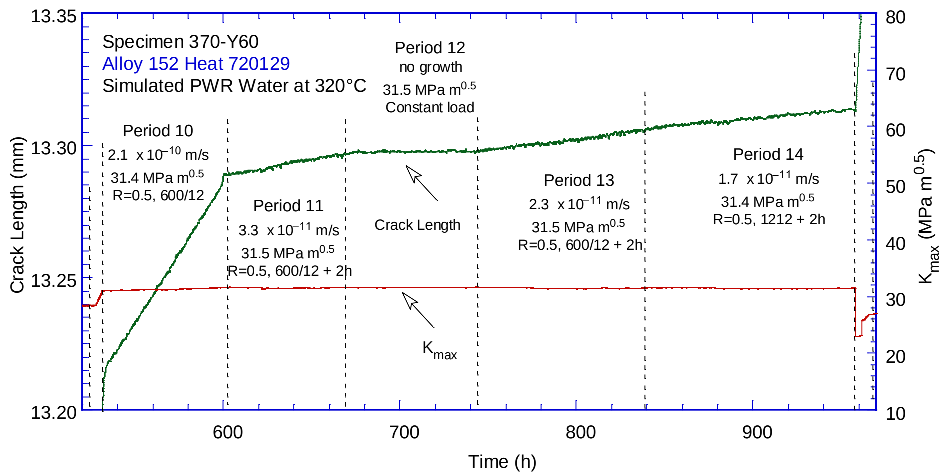

(c)

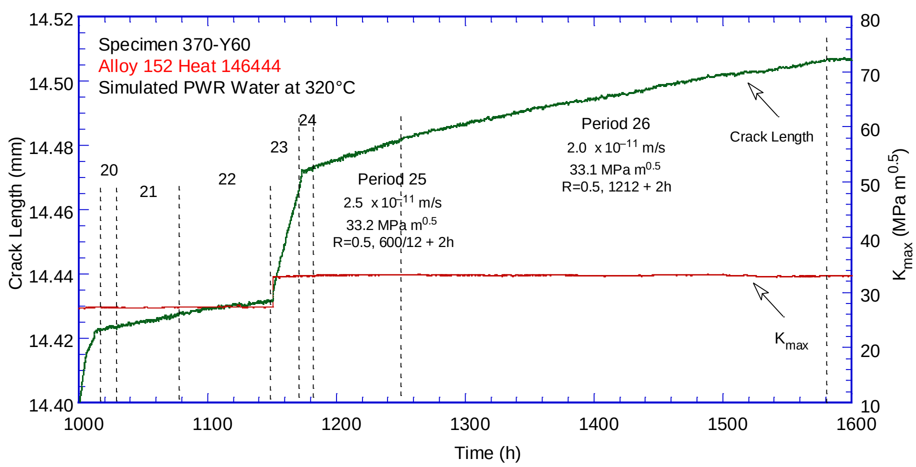

(d)

Figure 21 (cont.)

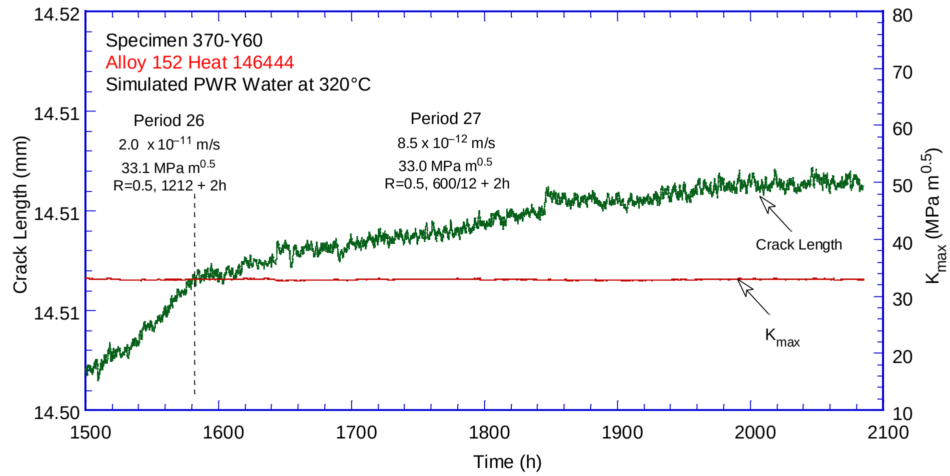

(e)

Figure 21 **(cont.)**

4 Discussion

This section provides summary of the aging effects in Alloy 152 and discusses the potential implications on performance. The testing results of aged alloys are discussed in the framework provided by the well-established fatigue and corrosion fatigue behavior for these alloys, as well as the industry-proposed disposition curves for crack growth.

4.1 Effects of aging on microstructure of Alloy 152

4.1.1 Long range ordering (LRO) in aged Alloy 152

Weldments – including weld butter layers – add several layers of complexity when compared to the base alloys: grain morphology, retained internal stress, segregation, precipitates, etc. All those factors may evolve with service time, as well as affect the formation of ordered phases such as LRO, for example, by altering the local diffusivity. Moreover, both microstructure and ordered phases can affect SCC.

The location of analysis within a weld is expected to play a role and potentially affect local diffusivity and outcomes of the microstructural investigations and analyses. Hence, as described in this report, a "finer" microstructural characterization by means of synchrotron X-ray was conducted in small, 0.2 mm - step line scans in the high-deformation regions of the weld root – covering areas spanning from the weld heat affected zone (HAZ) in Alloy 690 to the weld and weld butter on LAS. This investigation did not find evidence of LRO in any of the Alloy 152 heats aged at 370°C and 450°C to an equivalent of 60 years of service.

In summary, over the last two years, three Alloy 152 heats WC04F6, 720129, and 146444 – investigated as weldments and as weld butters - aged to 60 years of service equivalent did not show ordering. While LRO and its effect on SCC response is one of the main questions that this research is attempting to answer, it is important to keep in mind that the microstructural effects of thermal aging have been studied extensively in the past, leading to a comprehensive understanding of thermally-induced Cr carbide precipitation along grain boundaries [26], further resulting into an overall increase in hardness. From an SCC susceptibility standpoint, Cr carbide precipitation depletes Cr at grain boundaries [26], and thus could potentially decrease resistance to SCC. In essence, an increase in hardness, whether due to LRO formation or Cr-carbide precipitation, or both, can potentially have a negative effect on the SCC resistance, and hence needs to be investigated experimentally. The SCC CGR testing undertaken in this program and presented in this report addresses that need.

4.2 Effects of aging on crack growth response of Alloy 152

The SCC CGR test involved two aged Alloy 152 heats, 720129 and 146444. These were aged at 370°C for 74,808 h – equivalent to 60 years of service. The section summarizes and discusses the cyclic and SCC CGR results for the two heats.

4.2.1 Cyclic and SCC CGR response of aged Alloy 152 Heat 720129

Figure 22 summarizes the cyclic and SCC CGR data for aged Alloy 152 Heat 720129. Figure 22a presents the cyclic CGR data obtained on Alloy 152 heat 720129 in the as-welded and aged conditions. In the figure, the cyclic CGRs measured in the environment are plotted vs. the CGRs predicted in air under the same loading conditions for Ni-based weldments. In this representation, the environmental enhancement, i.e., the departure from the "1:1 diagonal" can be easily visualized. For comparison, the expected cyclic CGR curve for Alloy 182 weld was also included. Figure 22a shows that the cyclic CGRs in the mechanical fatigue regime (10^{-8}-10^{-7} m/s) are as expected, i.e., close to the first diagonal. Likewise, in the corrosion fatigue regime (10^{-11}-10^{-9} m/s), there is no difference between the aged and non-aged specimens. Also, unsurprisingly, at the lower end of the spectrum, the environmental enhancement of all Alloy 152 specimens is lower than the Alloy 182 curve – likely an effect of the higher Cr content than that of Alloy 182. Figure 22b presents the SCC CGR data for the aged Alloy 152 heat 720129 vs. stress intensity factor, K. In the non-aged condition, this alloy heat was only tested as a 1st layer butter on LAS [17], thus the SCC CGR data from the Cr-depleted (24-25%) version of this heat was deemed to be un-suitable for comparison in this context. Also, the proposed disposition curves for Alloys 182 [1] and 52/152 [2] are included in the figures. The SCC CGR data for the 60-year aged Alloy 152 heat 720129 is approximately a factor 20 higher than the EPRI MRP-386 [2] proposed disposition curve for high-Cr Ni-based weldments.

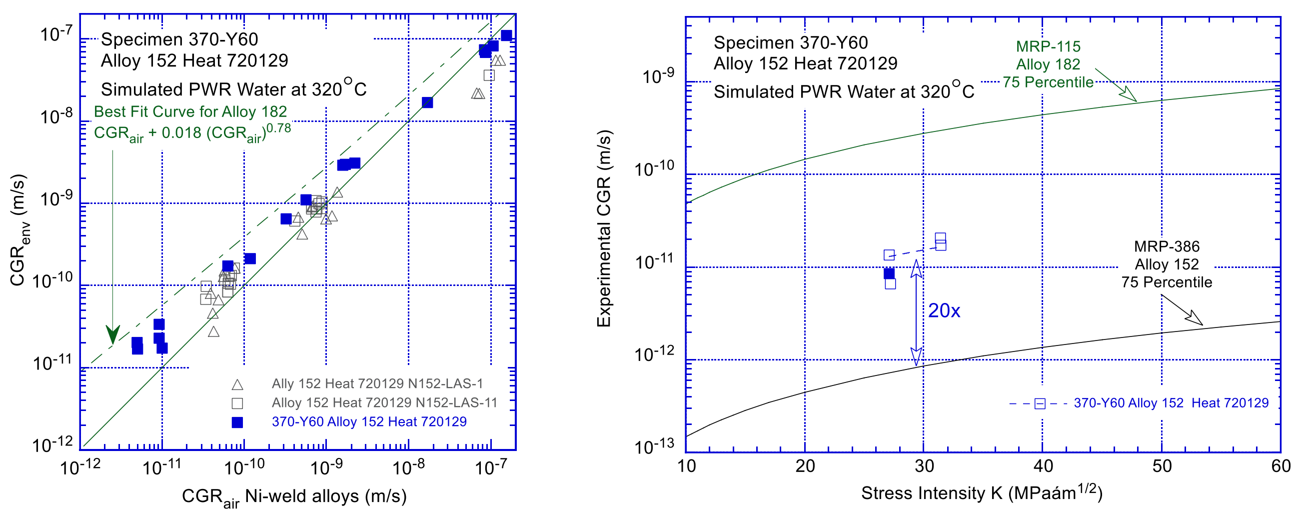

(a) (b)

Figure 22 (a) Cyclic CGRs measured in the environment vs. CGRs predicted in air under the same loading conditions, and (b) SCC CGRs for Alloy 152 weld heat 720129 in the as- received [16, 18], and aged conditions. For SCC CGRs, solid symbols represent measurements under constant load (CL) and open symbols represent measurements under periodic partial unloading (PPU) conditions. The proposed disposition curves for Alloys 182 [1] and 52/152 [2] are included.

4.2.2 Cyclic and SCC response of aged Alloy 152 Heat 146444

Figure 23 summarizes the cyclic and SCC CGR data for aged Alloy 152 Heat 146444, and provides a comparison with a non-aged version of this alloy. Alloy 152 Heat 146444 was only tested at ANL as a 2nd layer of weld butter deposited in LAS, with a 27% Cr concentration. However, the exact unaged version of this Alloy 152 heat was tested at GE CRD and the results are included in the EPRI MRP-386 database [2], and this dataset was deemed more suitable to compare against in order to evaluate the effect of aging. As such, Figure 23a presents the cyclic CGR data obtained on Alloy 152 heat 146444 in the non-aged and aged conditions. In the figure, the cyclic CGRs measured in the environment are plotted vs. the CGRs predicted in air under the same loading conditions for Ni-based weldments. In this representation, the environmental enhancement, i.e., the departure from the "1:1 diagonal" can be easily visualized. For comparison, the expected cyclic CGR curve for Alloy 182 weld was also included.

Figure 22a shows that, for the aged specimen, the cyclic CGRs in the mechanical fatigue regime (10^{-8}-10^{-7} m/s) are exactly as expected, i.e., along the first diagonal. In the corrosion fatigue regime (10^{-11}-10^{-9} m/s), there is no difference between the aged and non-aged specimens. Figure 22b presents the SCC CGR data for Alloy 152 heat 720129 in both aged and non-aged conditions vs. stress intensity factor, K. Also included are the aged Alloy 152 Heat 720129 data from the previous section, and the proposed disposition curves for Alloys 182 [1] and 52/152 [2] are included in the figures. The SCC CGR data for the 60-year aged Alloy 152 heat 720129 is approximately a factor 20 higher than the EPRI MRP-386 [2] proposed disposition curve for high-Cr Ni-based weldments, and a factor 50 higher than the SCC CGR data for the non-aged weldment.

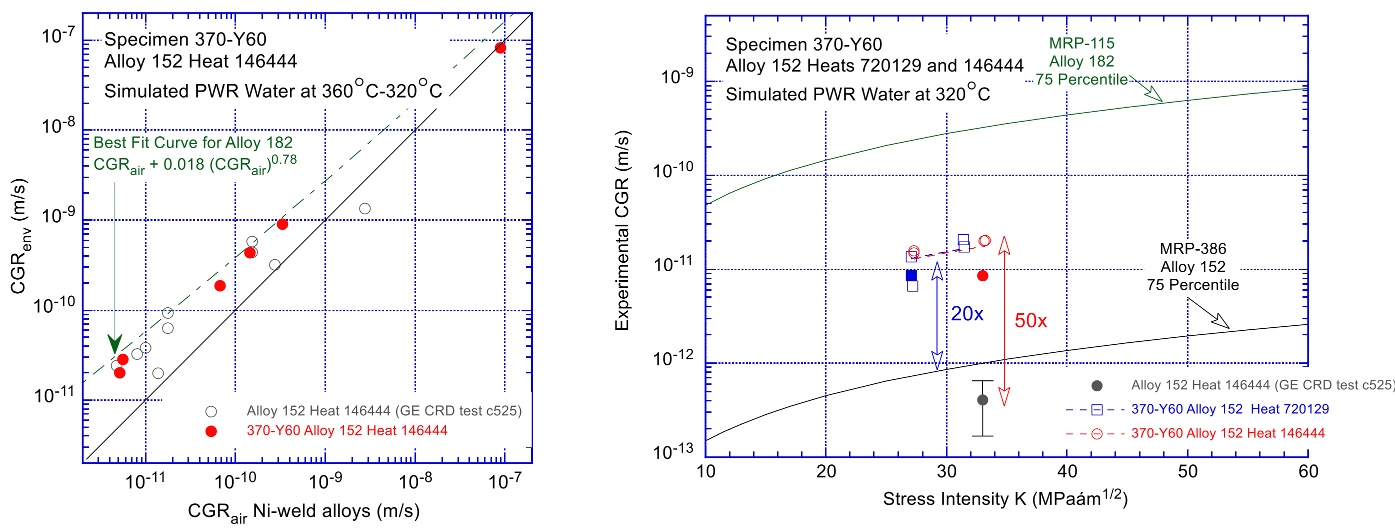

(a) (b)

Figure 23 (a) Cyclic CGRs measured in the environment vs. CGRs predicted in air under the same loading conditions, and (b) SCC CGRs for Alloy 152 weld heat 146444 in the as-received [16, 18], and aged conditions. For SCC CGRs, solid symbols represent measurements under constant load (CL) and open symbols represent measurements under periodic partial unloading (PPU) conditions. The proposed disposition curves for Alloys 182 [1] and 52/152 [2] are included.

As discussed previously, Alloy 152 Heat 146444 was tested at ANL as a 2nd layer of weld butter deposited in LAS, with a 27% Cr concentration measured along the crack path. Figure 24 attempts to capture and compare both effects – aging and Cr-dilution – for one heat of Alloy 152. As such, the figure includes SCC CGR data from the non-aged specimen tested at GE CRD, non-aged 2nd layer of butter, and specimen aged to 60 years of service. The comparison seems to suggest that aging to 60 years deteriorates SCC performance more than “mild” Cr dilution.

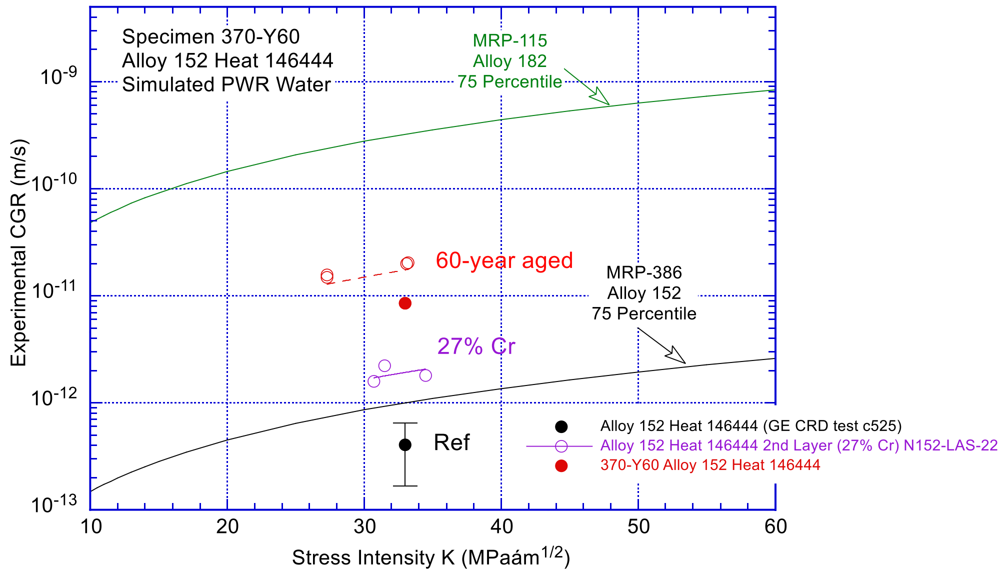

Figure 24 **SCC CGRs for Alloy 152 weld heat 146444 in the as- received [16, 18] and aged conditions as well as a 2nd layer of weld butter deposited in LAS, with a 27% Cr concentration measured along the crack path. The proposed disposition curves for Alloys 182 [1] and 52/152 [2] are included.**

5 Conclusions

The need for an assessment of the long term aging effects on the performance of Alloy 690 and associated weldments was identified as a research gap in the Light Water Reactor Sustainability (LWRS) stakeholders report for 2020 [9], being recognized as such by both industry [2, 10] and regulators [11]. The research undertaken in this program is addressing that gap. Specifically, the work focused on the microstructural evolution and the SCC response of Alloy 152 under accelerated thermal aging and conditions. The materials studied involved three heats of Alloy 152, aged at three different temperatures (370°C, 400°C and 450°C) for up to 75,000h. The conclusions of this research are as follows:

- For three heats of Alloy 152 weld, aging at 370°C and 450°C to 60 year equivalent service did not find evidence of LRO. Additional, detailed microstructural characterization by means of synchrotron X-ray conducted in small, 0.2 mm - step line scans in the high-deformation regions of the weld root – covering areas spanning from the weld heat affected zone (HAZ) in Alloy 690 to the weld and weld butter on LAS – substantiated these findings.
- While LRO was not found, the effect of aging on hardening is less clear. Aging to an equivalent of 60 years of service did not cause an increase in hardness, with the possible exception of the weld root area where hardness appears to increase slightly with aging. The aging temperature, 370°C or 450°C, does not seem to affect the findings. In absence of LRO, hardening is suspected to be due to thermally-induced Cr carbide precipitation. Carbide precipitation depletes Cr at grain boundaries [26], thus potentially decreasing the resistance to SCC. The SCC CGR testing undertaken in this program and presented in this report addresses that potential concern.
- Testing in a primary water environment of two Alloy 152 heats aged at 370°C to a 60-year service equivalent revealed a fatigue and corrosion fatigue crack growth responses similar to those measured on the un-aged alloy.
- The SCC CGR data for three 60-year aged Alloy 152 heats seem to show a deterioration of the SCC performance. A factor 20 vs. EPRI MRP-386 [2] proposed disposition curve appears to be a conservative estimate of that deterioration.

References

1. Materials Reliability Program: Crack Growth Rates for Evaluating Primary Water Stress Corrosion Cracking (PWSCC) of Alloy 82, 182, and 132 Welds (MRP-115), EPRI, Palo Alto, CA: 2004. 1006696.
2. Electric Power Research Institute, "Recommended Factors of Improvement for Evaluating Primary Water Stress Corrosion Cracking (PWSCC) Growth Rates of Thick-Wall Alloy 690 Materials and Alloy 52, 152, and Variants Welds (MRP-386)," Palo Alto, CA, 2017: 3002010756.
3. Young, G.A., Morton, D.S., Lewis, N. Morris, R., Pyle, J., Barnard, L., Najafabadi, R., Effect of Long Range Order on the Stress Corrosion Susceptibility of a Nickel-33 at% Chromium Alloy, Corrosion 72 2016 1433.
4. Marucco, A., Atomic Ordering in the Ni-Cr-Fe system, Mat. Sci. and Eng. A189 (1994) 267.
5. F. Delabrouille, D. Renaud, F. Vaillant, J. Massoud, Long range ordering of Alloy 690, in: 14th. Int. Conf. On Environmental Degradation of Materials in Nuclear Power Systems, 2009, pp. 888-894.
6. Brimbal, D., Joly, P., Benhamou, C., Thermal aging of Ni-Cr and Ni-Cr-Fe alloys to determine the potential for long-range ordering of Alloy 690 at PWR relevant temperatures, EPRI PWSCC Research Collaboration Meeting 2019, Tampa, Florida, December 4th, 2019.
7. Houtilainen, C., Ehrnstén, U., Ahonen, M., Hänninen, H., Effect of Thermal Aging on Microstructure and Hardness of Industrial Heats of Alloy 690, 19th. Int. Conf. On Environmental Degradation of Materials in Nuclear Power Systems, 2019.
8. Song, M., Yang, Y., Wang, M., Kuang, W., Lear, C.L., Was, G.S., Probing long-range ordering in nickel-base alloys with proton Irradiation, Acta Materialia 156 (2018) 446-462.
9. Light Water Reactor Sustainability Program Stakeholder Engagement Meeting Summary Report, INL/EXT-19-54520, February, 2020.
10. Burke, M., Coordination of EPRI Issue Programs' Research Activities with LWRS Materials Pathway Projects, LWRS Materials Research Pathway Stakeholder Engagement Meetings, August 18, 2020.
11. Collins, J., and Focht, E., Nickel-Based Alloy Crack Growth Rates, Industry / NRC Materials Programs Technical Information Exchange, August 11, 2021, ML21217A260.
12. Alexandreanu, B., Chen, Y., Zhang, X., and W. Y. Chen, "Effect of Thermal Aging and Irradiation on Microstructure and Crack Growth Response in Alloy 690," ANL/LWRS- 21/1, September 2021.
13. Alexandreanu, B., Chen, Y., Zhang, X., and W. Y. Chen, "Effect of Thermal Aging and Irradiation on Microstructure and Crack Growth Response in Alloy 152 Weld," ANL/LWRS- 22/2, September 2022.
14. Material Documentation Report for Consumers Power Midland (620-0012-51) and TMI-2 (620-0006-51) Reactor Vessel Lower Head Material, The Babcock & Wilcox Company, BAW-2071, January 1989.
15. Dunn, D., Alexandreanu, B., Toter, W., "Shielded Metal Arc Welding Parameters for Primary Water Stress Corrosion Cracking Test Materials," Technical Letter Report ML13171A113, June 2013.
16. Alexandreanu, B., Y. Yang, Y. Chen, and W. J. Shack, "Stress Corrosion Cracking in Nickel-Base Alloys 690 and 152 Weld in Simulated PWR Environment - 2009," NUREG/CR–7137, ANL–10/36, June 2012.
17. Alexandreanu, B., Chen, Y., Natesan, K., and Shack, "Primary Water Stress Corrosion Cracking of High-Chromium, Nickel-Base Welds Near Dissimilar Metal Weld Interfaces," NUREG/CR–7226, ANL–16/10, January 2018.
18. Alexandreanu, B., Chen, Y., Natesan, K., and Shack, "Primary Water Stress Corrosion Cracking of High-Chromium, Nickel-Base Welds - 2018," NUREG/CR–7276, 2021.

19. Choi, K.J., Kim, J.J, Bong, H.L., Bahn, C.B., Kim, J.H., Effects of thermal aging on microstructures of low alloy steel–Ni basealloy dissimilar metal weld interfaces, Journal of Nuclear Materials 441 (2013) 493-502.
20. Yoo, S.C., Choi, K.J., Bahn, C.B., Kim, S.H., Kim, J.Y., Kim, J.H., Effects of thermal aging on the microstructure of Type-II boundaries in dissimilar metal weld joints, Journal of Nuclear Materials 459 (2015) 5-12.
21. B. Alexandreanu, B. Capell and G.S. Was, Combined Effect of Special Grain Boundaries and Grain Boundary Carbides on IGSCC of Ni-16Cr-9Fe-xC Alloys, *Mat. Sci. and Eng.* A 300 (2001) 94.
22. Gwalani, B., Alam, T., Miller, C., Rojhirunsakool, T., Kim, Y.S., Kim, S.S., Kaufman, M., Ren, Y., and Banerjee, R., (2016). Experimental investigation of the ordering pathway in a Ni-33 at.%Cr alloy. Acta Materialia. 115. 372-384. 10.1016/j.actamat.2016.06.014.
23. American Society for Testing and Materials, "Standard Test Method for Measurement of Fatigue Crack Growth Rates," ASTM E647-08, DOI 10.1520/E0647-08, West Conshohocken, PA, 2008.
24. American Society for Testing and Materials, "Standard Test Method for Determining a Threshold Stress Intensity Factor for Environment-Assisted Cracking of Metallic Materials," ASTM E1681-03, DOI 10.1520/E1681-03R08, West Conshohocken, PA, 2008.
25. Electric Power Research Institute, "PWR Primary Water Chemistry Guidelines," Volume 1, Revision 4, EPRI, Palo Alto, CA, 1999.
26. Angeliu, T.M., and Was, G.S., Behavior of grain boundary chemistry and precipitates upon thermal treatment of controlled purity Alloy 690, Metall. Trans. A 21A, 2097 (1990).
27. Ruther, W. E., W. K. Soppet, and T. F. Kassner, "Corrosion Fatigue of Alloys 600 and 690 in Simulated LWR Environments," NUREG/CR-6383, ANL-95/37, April 1996.
28. Ruther, W. E., W. K. Soppet, T. F. Kassner, and W. J. Shack, "Environmentally Assisted Cracking of Alloys 600 and 690 in Simulated LWR Water," in Environmentally Assisted Cracking in Light Water Reactors, Semiannual Report, January 1998-July 1998, NUREG/CR-4667, Vol. 26, ANL-98/30, pp. 25-32, March 1999.
29. Chopra, O. K., W. K. Soppet, and W. J. Shack, "Effects of Alloy Chemistry, Cold Work, and Water Chemistry on Corrosion Fatigue and Stress Corrosion Cracking of Nickel Alloys and Welds," NUREG/CR-6721, ANL-01/07, April 2001.
30. Alexandreanu, B., O. K. Chopra, and W. J. Shack, "Crack Growth Rates of Nickel Alloys from the Davis-Besse and V. C. Summer Power Plants in a PWR Environment," NUREG/CR–6921, ANL–05/55, November 2006.
31. Alexandreanu, B., O. K. Chopra, and W. J. Shack, "Crack Growth Rates of Nickel Alloy Welds in a PWR Environment," NUREG/CR–6907, ANL–04/3, May 2006.

This page intentionally left blank

Nuclear Engineering Division
Argonne National Laboratory
9700 South Cass Avenue, Bldg. 208
Argonne, IL 60439

www.anl.gov